

Heavy elements and electromagnetic transients from neutron star mergers

Stephan Rosswog^{1,2} & Oleg Korobkin³

¹Hamburger Sternwarte, University of Hamburg, Gojenbergsweg 112, 21029 Hamburg, Germany;
Email Address: stephan.rosswog@uni-hamburg.de

²Department of Astronomy & Oskar Klein Centre, Stockholm University, SE-106 91, Stockholm, Sweden

³Center for Theoretical Astrophysics, Los Alamos National Laboratory, Los Alamos, NM 87545, USA
Email Address: korobkin@lanl.gov

Keywords: *r*-process, neutron stars, gravitational waves, kilonovae

Compact binary mergers involving neutron stars can eject a fraction of their mass to space. Being extremely neutron rich, this material undergoes rapid neutron capture nucleosynthesis, and the resulting radioactivity powers fast, short-lived electromagnetic transients known as kilonova or macronova. Such transients are exciting probes of the most extreme physical conditions and their observation signals the enrichment of the Universe with heavy elements. Here we review our current understanding of the mass ejection mechanisms, the properties of the ejecta and the resulting radioactive transients. The first well-observed event in the aftermath of GW170817 delivered a wealth of insights, but much of today’s picture of such events is still based on a patchwork of theoretical studies. Apart from summarizing the current understanding, we also point out questions where no consensus has been reached yet, and we sketch possible directions for the future research. In an appendix, we describe a publicly available heating rate library based on the WinNet nuclear reaction network, and we provide a simple fit formula to alleviate the implementation in hydrodynamic simulations.

1 Introduction

The basic nuclear physics of the rapid neutron capture, or “*r*-process”, responsible for about half of the elements heavier than iron, has been laid out already in the 1950ies of the last century.^[1,2] The astrophysical site where it actually happens, however, has remained a mystery for the decades to come. Throughout this time, the vast majority of the research community considered core-collapse supernovae as the most likely production site, despite the fact that such models were perpetually struggling to reach the 3rd *r*-process or “platinum” peak around the nucleon number $A = 195$. For some time there was hope to produce such elements in high-entropy winds driven from newborn proto-neutron stars,^[3–6] but a slew of more recent supernova investigations does not support the emergence of the very large entropies that would be needed,^[7–13] and today core-collapse supernovae are considered to contribute at best to the light *r*-process elements. More extreme, and likely more rare, stellar explosions that magnetorotationally launch jets,^[14–21] and also collapsars^[22–27] have been suggested as possible sites of heavy *r*-process, but while this is physically plausible, it is currently not clear, how robustly nature realizes the specific conditions^[16,27–29] that are needed for heavy *r*-process in jet- and accretion-disk outflows and how large the overall contribution from such sources is on a cosmic scale.

The Milky Way is enriched by *r*-process elements at an average rate of roughly $1M_{\odot} \text{ Myr}^{-1}$,^[30–32] but this could, in principle, be the result of either frequent, low-yield (e.g. common core-collapse supernovae) or rare, high-yield events (e.g. neutron star mergers). A number of independent arguments ranging from large variance of *r*-process matter in metal-poor stars and ultra-faint dwarf galaxies^[33–36] to deep-sea floor ^{244}Pu ^[37,38] all point to very rare events ejecting on average several percent of a solar mass and occurring at $\sim 1/1000$ of the core-collapse supernova rate, see e.g. Ref. [32,39–41]

for more detailed discussions of this topic. In other words, also these arguments strongly disfavour regular supernovae as major source, consistent with modern supernova simulations. Instead, they favor substantially rarer events such as neutron star mergers or rare breeds of stellar explosions.

The idea that decompressed neutron star matter could be a promising *r*-process site was discussed by Lattimer and Schramm in the context of neutron star black hole mergers^[42,43] and further discussed in Symbalisty and Schramm,^[44] this time considering neutron star mergers. These ideas were met with scepticism, both because no gravitational-wave driven merger had, of course, been observed at the time, and because it is non-trivial to unbind matter from a neutron star: the gravitational binding energy exceeds 150 MeV/baryon. The idea of decompressing neutron star matter gained further credibility after the discussion paper of Eichler et al.,^[45] which placed neutron star mergers in a broader astrophysical perspective and connected them not only with nucleosynthesis, but also with neutrino and gamma-ray bursts. The first hydrodynamic plus nucleosynthesis calculations^[46–48] showed that neutron star mergers eject $\sim 1\%$ of a solar mass per event, that these extremely neutron-rich ejecta effortlessly reach the platinum peak and beyond, and that, when folded with the estimated merger rates, the produced *r*-process mass is enough for neutron star mergers being the major (or maybe even the only) *r*-process source.

While already these studies made a strong case for neutron star mergers as important *r*-process site, the picture has become substantially more detailed in recent years. On the one hand more ejecta channels were identified: dynamic ejecta launched by shocks (rather than tidal torques),^[49–53] neutrino- and magnetically driven winds,^[54–58] (magnetohydrodynamic and nuclear) unbinding of accretion tori,^[29,59–64] and last but not least, by viscous processes^[58,65,66] in the remnant. On the other hand, it was realized that these differ-

arXiv:2208.14026v2 [astro-ph.HE] 13 Oct 2022

ent ejection channels go along with different weak interaction histories and therefore the ejecta have different neutron-to-proton ratios. This is usually quantified via the “electron fraction” $Y_e = n_e/(n_n+n_p) = n_p/(n_n+n_p)$, where the indexed n ’s refer to the number densities of electrons, neutrons and protons. Under the conditions realized in neutron star mergers, Y_e has *the* decisive impact: the resulting r -process abundance pattern changes rather abruptly^[67–69] around $Y_e \approx 0.25$, with lower values producing “heavy r -process” with nucleon numbers $A > 130$ while values above this threshold produce only light “ r -process” ($A < 130$).

Tidal dynamical ejecta are hardly heated and expand rapidly, so that weak interactions have no chance to substantially change the ejecta’s number of neutrons and protons and they keep their original, cold β -equilibrium electron fraction $Y_e \sim 0.05$ and therefore produce strong r -process along the lines found in Ref. [48]. Shock-heated dynamic ejecta, in contrast, are substantially heated and, although they escape with large velocity, their electron fraction may be substantially altered. Neutrino-driven winds start out with low velocities in an environment flooded with neutrinos, and as they become secularly driven out of the remnant’s gravitational pull, they have plenty of time to change their neutron-to-proton ratio. The detailed electron fractions in most of the more recently identified ejection channels are currently still unsettled questions,^[29, 56, 62–64, 70] but it seems clear that a much broader range than initially thought is realized in nature and several studies found neutron star mergers to produce the whole range of r -process elements^[71–73] rather than only the main r -process elements with $A > 130$ as found in the first study of Ref. [48].

A number of excellent reviews related to the broad topic of our paper have appeared in recent years. For example, with a strong focus on r -process, there are the reviews of Ref. [40, 74, 75], Ref. [32, 76–78] discusses in detail the electromagnetic counterparts of compact binary mergers, while Ref. [79] and Ref. [80] focus more on the merger itself.

2 The theoretical picture

The first detection of a gravitational wave signal from a neutron star merger^[81] (GW170817) and its subsequent electromagnetic transient^[82] (AT2017gfo) has overall provided a strong confirmation of the theoretical picture that had been developed by the theoretical astrophysics community over the preceding two decades. Here we will provide a short overview over the, observationally informed but predominantly theoretical, picture that has emerged over the years. It is worth mentioning that none of the studies that this picture is based upon contains all the relevant physics ingredients to sufficient accuracy, and no study can claim full numerical convergence of the post-merger stage. What we will present is also idealized in the sense that what we list below as separate channels may in reality occur in a concerted way. For example, winds may be driven by the combined action of neutrino-absorption and the dissipation of magnetic fields in a “hot corona” above the disk. In line with the topic of this article, we will focus on the ejecta and the electromagnetic emission they cause. But before we get there, we have to briefly summarize the dynamical

evolution of a neutron star merger and outline different pathways for its further evolution.

2.1 Dynamical evolution

The post-merger multi-messenger signatures –gravitational waves, neutrino emission, mass ejection and electromagnetic emission– are closely tied to the fate of the merger remnant. Binary systems with masses $> 2.8 M_\odot$ can collapse on a dynamical time scale (“no bounce”) to black holes, with the exact threshold mass depending on the equation of state (EOS).^[50, 83–86] Black holes formed in such a prompt collapse are not surrounded by massive disks unless the mass ratio of the binary, q , deviates substantially from unity. It takes $q \lesssim 0.8$ to form disks of moderate mass ($> 0.01 M_\odot$),^[87–89] for even more extreme mass ratios the tidal shredding of the secondary neutron star can still lead to sizeable disk masses.^[85] For the close-to-equal mass case there are hardly any ejecta expected and such systems may be electromagnetically undetectable. For mass ratios smaller than about 0.8 the ejecta mass can exceed $10^{-3} M_\odot$ in a prompt collapse.

Out of the 13 galactic neutron star binaries with total masses published in Ref. [90], 11 have a mass below $2.8 M_\odot$. It is therefore likely that the majority of neutron star binaries goes at least temporarily through a phase where a massive neutron star is present. This has a major impact since the central remnant can keep emitting gravitational waves, shed mass into a torus, eject matter, and provide a strong central neutrino source that can modify the neutron-to-proton ratio. For this case with a central neutron star remnant, the amount of ejecta is strongly dependent on the EOS. If the EOS is stiff, neutron stars of a given mass have larger radii (than for a soft EOS) and therefore the tidal effects are larger, and the merger occurs earlier, at larger orbital separations, and with smaller orbital velocities. In addition, the sound speed of stiff EOSs is larger, so it is more difficult to shock the neutron star matter. Therefore, shock heating is not very efficient, and the post-merger oscillations are less violent, so not much mass is ejected dynamically. Softer equations of state, in contrast, lead to a longer inspiral, larger velocities at contact, stronger shocks, more violent post-merger oscillations and therefore larger amounts of dynamically ejected mass. However, even for soft EOSs the dynamic ejecta mass from equal-mass binaries is typically only a few times $\sim 10^{-3} M_\odot$,^[52, 91–93] while unequal-mass binaries produce larger amounts of ejecta with a more pronounced tidal contribution and lower electron fractions. Extreme cases with very large mass ratios and (implausibly) stiff EOSs¹ can reach ejecta masses of $\sim 0.06 M_\odot$ of tidal ejecta.^[94]

2.2 Ejection channels

We sketch in Figure 1 possible post-merger configurations together with various ejection channels. The left half of the figure illustrates the case where a central neutron star survives, the right is a sketch of the configuration after the central neutron star has collapsed into a black hole or, alternatively, it could be produced in the merger of a neutron star with

¹The used MS1b EOS is disfavoured by the limits on tidal deformability.^[81]

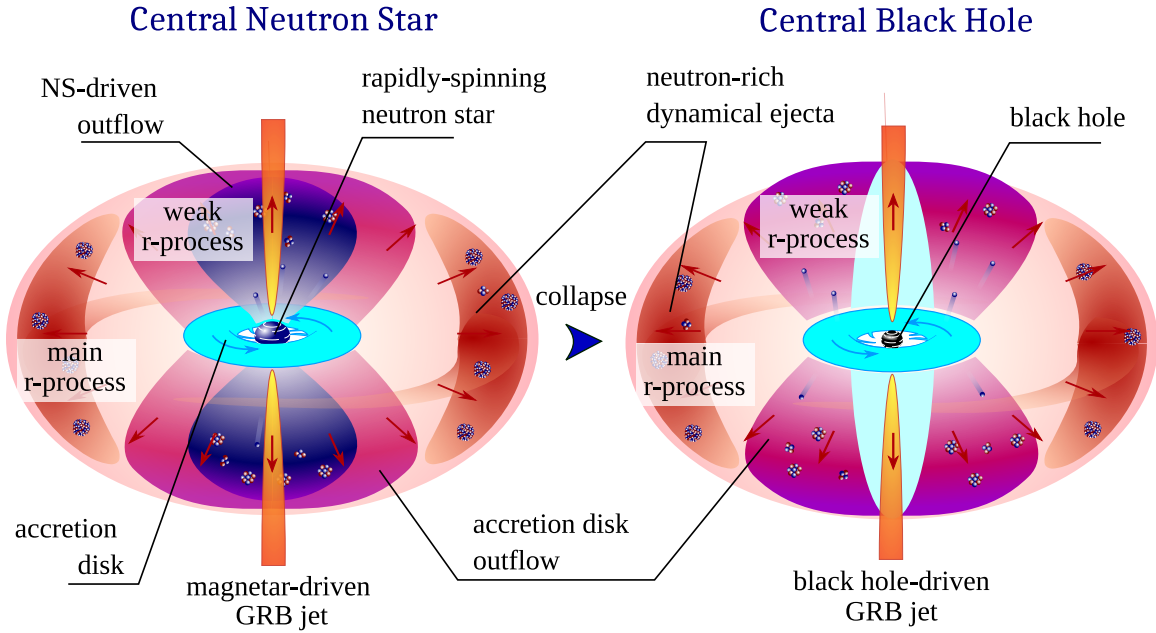


Figure 1: Sketch of potential post-merger remnant structures.

a stellar-mass black hole. Keep in mind that neutron star mergers with nearly equal masses may not form any torus of significant mass. If a neutron star survives either temporarily or indefinitely, it will be very highly rotating and likely have a beyond-magnetar field strength.^[95–97] This may continuously inject a large flux of energy into the remnant which could potentially lead to electromagnetic light curves that are very different from the case where the central object is a black hole.^[98]

As alluded to above, the number of known ejecta channels has substantially increased in recent years, and we group them here broadly into “dynamic ejecta”, “winds”, and “torus ejecta”, which we discuss separately below.

2.2.1 Dynamic ejecta

The historically first identified ejection channel are so-called dynamic ejecta that are launched on a dynamical time scale (~ 1 ms) at merger. The ejecta of equal mass systems are dominated by *shock-driven* ejecta, while with decreasing mass ratio q the contribution from *tidal ejecta* becomes more and more important. The shock-driven ejecta result from both matter being shocked at the interface between the merging stars, and from strong post-merger pulsations of the remnant when outward travelling sound waves steepen into shocks as they pass through matter of decreasing density (and therefore decreasing sound speeds). Since this matter becomes heated to temperatures of a few MeV, where the weak interaction time scales compete with the dynamical ones, its electron fraction can increase substantially by both positron captures, $n + e^+ \rightarrow p + \bar{\nu}_e$, and neutrino absorptions, $n + \nu_e \rightarrow p + e^-$. The latter process, however, needs some time to “ramp up” since the neutrino luminosities only reach large values once a substantial torus has been assembled around the central object which typically takes ~ 5 ms. Tidal ejecta, in contrast, usually do not experience shocks and are therefore ejected with their pristine, neutron star electron fraction of $Y_e \sim 0.05$

(but see the discussion in Sec. 4.2.1). The detailed ejecta properties depend on the total mass, the mass ratio q and the equation of state, but one can expect a broad distribution of Y_e between ~ 0.05 and 0.4 .^[52, 71, 99] The total amount of dynamic ejecta found in simulations ranges from $\sim 10^{-4}$ to $\sim 10^{-2} M_\odot$ ^[47, 52, 91–94, 99–101] with soft equations of state typically ejecting more matter than stiff ones.

The average ejecta velocities are in a range between $\sim 0.15c$ to $\sim 0.3c$,^[52, 91, 93, 99] but for specific cases² they can reach $\sim 0.4c$.^[92] Many groups have found small amounts of ejected matter (the exact numbers are rather uncertain, but roughly of order $\sim 10^{-5} M_\odot$) that reach asymptotic velocities in excess of $0.5c$.^[52, 91–93, 102–105] While none of the groups can claim full numerical convergence of the properties of this small amount of mass from 3D simulations, it seems increasingly clear that such a high-velocity tail does exist. As Fig. 3 suggests, this high-velocity component is (at least partially) due to shock-heated matter from the interface between the two neutron stars. If indeed such a high-velocity component is present, the ejecta should contain a significant fraction of free neutrons at freeze-out, and their decay should cause an early blue/UV transient on a time scale of several minutes to an hour.^[103, 106] Moreover, such a high-velocity component would have a strong effect on the shock breakout signal^[107] and it could additionally cause synchrotron emission many months after a neutron star merger.^[108–111]

The majority of simulation studies has focussed on irrotational binary systems. This is because the combination of low viscosity in the neutron star matter and the very short time (~ 0.01 s) the binary components interact tidally do not allow for a substantial tidal spinup.^[112, 113] Nevertheless, there might be some residual stellar spins left at merger and a few studies have explored their impact. In extreme cases, spins can enhance the dynamic ejecta (and disk) masses by more

²These latter simulations use the conformal flatness approximation to General Relativity.

than an order of magnitude^[114] and they can impart asymmetries to the ejecta and kicks to the central remnants.^[115,116]

2.2.2 Winds

On a time scale exceeding the dynamical one, various processes can unbind matter from the accretion disk³. First, and especially for the likely common case that a central neutron star survives at least temporarily, energy deposition by neutrino absorption can inflate the disk vertically and can drive quasi-spherical outflows on time scales of ~ 100 ms.^[52,54,55] Since this matter is exposed to intense neutrino irradiation, and the time scales are relatively long, its neutron-to-proton ratio can change substantially and will, starting from the pristine Y_e -value < 0.1 , evolve towards an equilibrium value^[120,121] of

$$Y_e^{\text{eq}} \approx \left(1 + \frac{L_{\bar{\nu}_e} W_{\bar{\nu}_e} \epsilon_{\bar{\nu}_e} - 2\Delta + 1.2\Delta^2/\epsilon_{\bar{\nu}_e}}{L_{\nu_e} W_{\nu_e} \epsilon_{\nu_e} + 2\Delta + 1.2\Delta^2/\epsilon_{\nu_e}} \right)^{-1}, \quad (1)$$

where the L_i denote the neutrino luminosities, $W_i = 1 + \eta_i \langle E_i \rangle / m_b c^2$ are weak magnetism correction factors with $\eta_{\nu_e} = 1.01$ and $\eta_{\bar{\nu}_e} = -7.22$, $\Delta = (m_n - m_p)c^2 \approx 1.29$ MeV and ϵ_i are the ratios between the average squared neutrino energy and the average neutrino energies (typically $\epsilon_\nu \approx 1.2E_\nu$). For the typical neutrino field properties reached in a merger, this equilibrium value is ~ 0.4 , see e.g. Fig. 23 in Ref. [41]. It is, however, by no means guaranteed that during the dynamic evolution of the remnant the ejecta will reach this equilibrium value. Numerical studies show that a broad distribution of electron fractions between ~ 0.1 and ~ 0.4 and, for long-lived central remnants, ejecta masses of $\sim 0.01 M_\odot$ are reached.^[52,54,55,122]

Apart from this neutrino-driven wind, the accretion process itself will unbind some material: as neighbouring, quasi-circular disk segments couple viscously, angular momentum is removed from the inner regions, thus allowing accretion, and it is transferred to the outer portions of the flow which, by being continuously fed with angular momentum, can expand quasi-spherically to infinity. Another, likely more efficient mechanism is realized by the so-called ‘‘spiral wave winds’’.^[53,70] They emerge in cases where the central remnant does not collapse quickly to a black hole and instead forms non-axisymmetric bar modes that continuously pump angular momentum into the surrounding accretion disk. As a result, matter becomes unbound, predominantly in the orbital plane, in the form of a spiral wave. This process continues until either the central remnant collapses or the bar mode is dissipated (by gravitational waves or other mechanisms).

If large-scale, ordered magnetic fields emerge in the remnant, they also can drive outflows. Both the spiral-wave and the magnetically driven winds are expected to reach masses of $\sim 0.01 M_\odot$, asymptotic velocities of 0.1–0.2c and have electron fractions in excess of the critical value of ≈ 0.25 .^[67,68] With

³Sometimes the word ‘‘disk’’ is reserved for geometrically thin accretion disks and ‘‘torus’’ for thicker matter configurations that are thermally ‘‘puffed up’’ because they cannot efficiently cool on a dynamical time scale. A good fraction of the post-merger accretion may proceed in a neutrino-cooled regime, so one may argue that ‘‘disk’’ might be more appropriate. However, we do not want to distinguish in our wording between the different cases and simply use the word ‘‘torus’’.

such properties, they are viable candidates^[70,123] to explain the early, blue kilonova component of the transient that followed GW170817, see e.g. Ref. [124–126]. Depending on magnetic field strength and rotational period, magnetized winds can reach larger velocities^[127] than spiral wave winds which might potentially help to explain the large inferred velocities of the blue component of GW170817.

2.2.3 Torus ejecta

While the above discussed ejecta components could potentially provide masses close to what was estimated for GW170817 (but keep in mind that the current estimates could be too large due to the assumption of sphericity^[128]), it is worth noting that the winds (neutrino-, magnetic- and spiral wave-driven) are all candidates for the blue kilonova component. At the same time, the red component was estimated in some studies to be the result of as much as $\sim 0.04 M_\odot$ of matter with a rather low average velocity of $\sim 0.1c$ (e.g. Ref. [129]). Dynamic ejecta are the only channel discussed so far that could produce a red signal, but they fall short in producing this large amount of mass and their average velocity is substantially in excess of the inferred value of 0.1c. A channel that potentially can provide ejecta with such properties is the late-time (~ 1 s) unbinding of the accretion disk^[29,59,60,62–64] (but see the discussion below for possible caveats).

The torus ejection mechanism is a combination of two effects: as the disk expands viscously, it cools, and, once the temperature drops below $\sim 5 \times 10^9$ K, the neutrons and protons that constitute the disk material combine into α -particles, releasing 7.1 MeV/nucleon. From the location where this happens, this energy release alone would launch ejecta with asymptotic velocities of $\sim 0.05c$. Detailed numerical simulations of the accretion of thick disks (initially in equilibrium) that account for the assembly of nucleons into α -particles and the evolution of magnetic fields,^[29,62] find that steady-state MHD turbulence develops strong magnetic fields in the disk and generates a hot disk corona that, helped by the assembly of nucleons into α -particles, launches powerful thermal, quasi-spherical outflows. Via this mechanism up to $\sim 40\%$ of the initial disk mass can become unbound with the outflows reaching asymptotic bulk velocities⁴ of $\sim 0.1c$. Thus, a typical accretion disk from a neutron star merger with $\sim 0.1 M_\odot$ as initial disk mass, would plausibly produce the masses and outflow velocities that have been inferred for the red component.

Interestingly, at the expected accretion rates (which are those that are needed to launch a GRB), the inner parts of the disk mid-plane regulate themselves into a state of mild electron degeneracy which creates a negative feedback cycle resulting in electron fraction values of $Y_e \approx 0.1$ in the inner disk regions.^[60,62,130–133] This is interesting for at least two reasons. First, it deviates from the maybe naïve expectations that a hot, but initially very neutron-rich disk should increase all of its electron fraction rapidly (in some parts of the disk this happens, though), and it provides a rather robust mechanism to produce low- Y_e material. If the electron fraction of this material should rise only mildly during the

⁴The outflows also contain high-velocity tails up to $\sim 0.5c$; J. Miller, private communication.

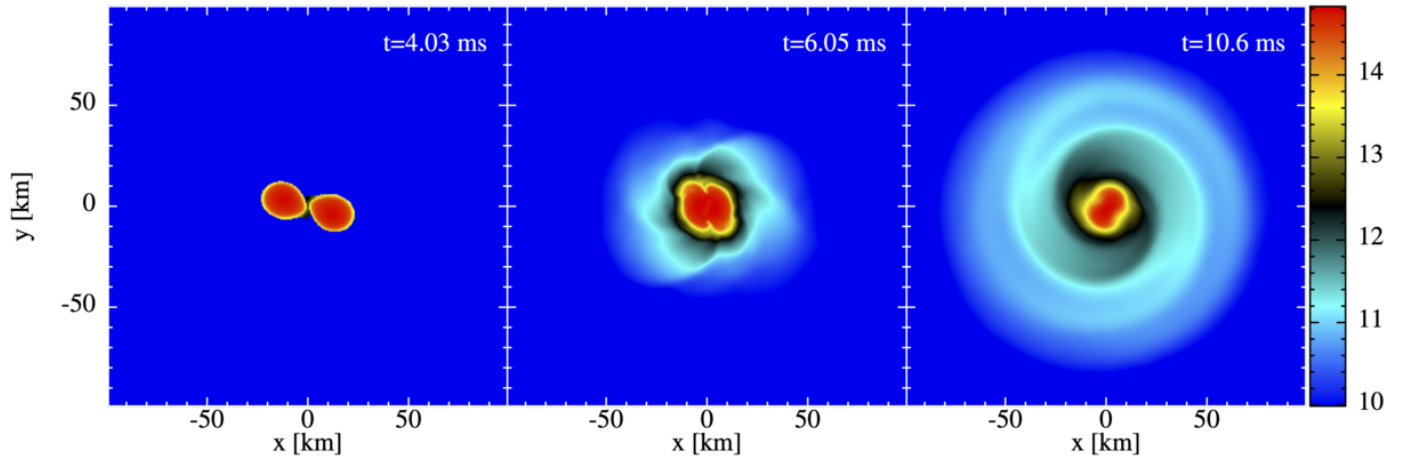


Figure 2: Simulated merger of a $2 \times 1.3 M_{\odot}$ neutron star binary with the MPA1 equation of state. The simulation was performed with the Lagrangian Numerical Relativity code SPHINCS_BSSN.^[93, 117–119]

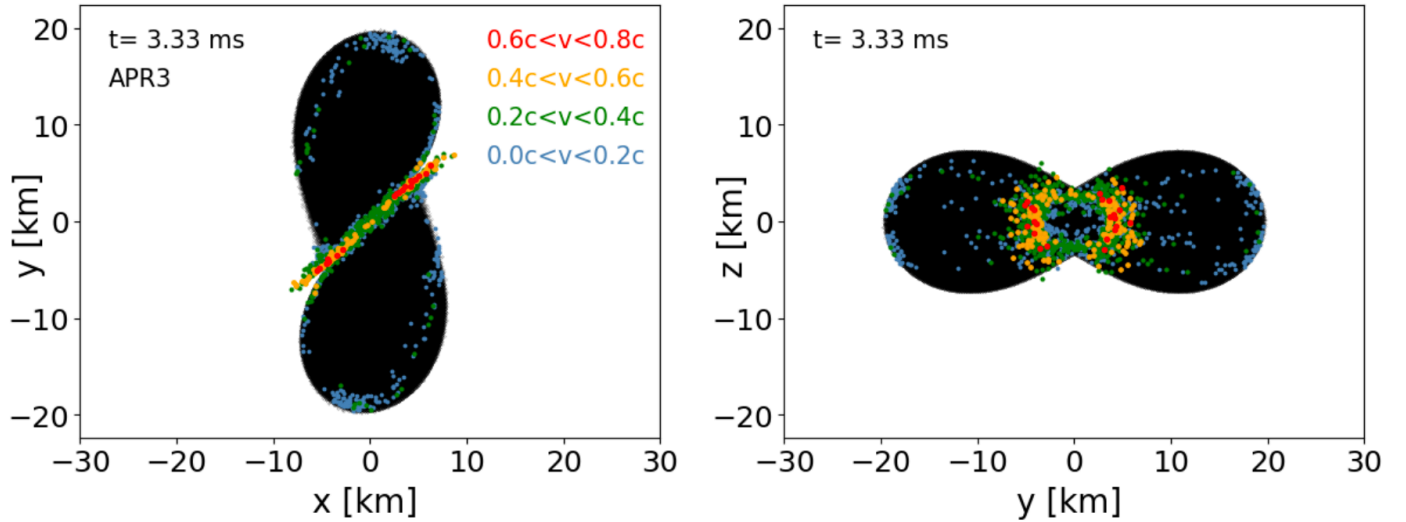


Figure 3: Particle positions (black) during the time of merger ($2 \times 1.3 M_{\odot}$, APR3 equation of state). Overlaid are the positions of particles that are finally ejected with asymptotic velocities v_{∞} between 0 and $0.2c$ (blue), between 0.2 and $0.4c$ (green), between 0.4 and $0.6c$ (orange) and above $0.6c$ (red). The simulation was performed with the Lagrangian Numerical Relativity code SPHINCS_BSSN.^[93, 117–119]

ejection process, disk ejecta below the critical value $Y_e^{\text{crit}} \approx 0.25$ ^[67,68] for heavy r -process production can emerge. Second, there is an interesting potential connection to observed “actinide boost stars”. These are stars that have thorium- or uranium-to-europium ratios that substantially exceed the solar values.^[134–136] Nuclear parameter studies^[137–139] that explored under which conditions such “actinide boosts” can occur found that they require a rather narrow electron fraction range of $0.1 < Y_e < 0.15$. The only astrophysical “engines” that we are aware of that have good physical reasons to preferentially produce electron fractions in this range are such accretion disks. It has therefore been speculated^[41] that such disks might be the sites that produce the abundances for the “actinide boosts” in stars. If true, this would also connect actinide boost stars to the sources of gamma-ray bursts.

The picture of accretion disks ejecting low electron fraction material, being a good candidate for the red kilonova component of GW170817 and a major production site of 3rd-peak r -process, however, is not undisputed. Recent studies by Miller and collaborators^[27,64,140] evolving accretion disks in fixed Kerr spacetimes employing Monte Carlo neutrino transport comes to a different conclusion, namely that the ejecta should be predominantly above $Y_e = 0.25$ and therefore produce a blue kilonova. Given the (physical and numerical) complexity of the challenge, it is not entirely surprising that at this early stage of studying such 3D-GRMHD accretion disks with neutrino cooling the results do not agree. However, it is worth keeping in mind that the studies of Siegel and collaborators and Miller and collaborators investigate different physical parameters and use different approximations of the involved physics, in particular in their treatment of neutrinos. The latter has been studied in detail by Ref. [141], though not in GR, but using Newtonian α -disk/ MHD simulations with a pseudo-potential for the black hole.^[142] The authors point out the importance of the initial disk electron fraction (of which some parts can become unbound without much neutrino interactions), the substantial differences between an α -disk and an MHD treatment, but they also stress that plausible simplifications such as neglecting electron masses and the mass difference between neutrons and protons can have an impact. It seems in particular that neutrino absorption effects become important already for disks of moderate masses ($> 0.01 M_\odot$)^[141,143] and that relatively simple treatments such as leakage schemes or an M1-approach may underestimate the related effects. To the best of our knowledge, the issue of the composition of torus ejecta is at the time of writing not yet settled and possible solutions include the possibility that all the differences are due to the neutrino treatment, but it could also be that different physical parameters (black hole masses and spins, disk masses, isolated black hole disk systems as they may emerge after a neutron star merger vs continuously fed systems as they may emerge in collapsar case) can lead to different physical outcomes. Clearly, substantially more work is needed to settle this issue in the future.

In passing, we want to stress that *if* the resolution of this issue should be the neutrino transport and the torus ejecta should be above $Y_e = 0.25$ and *if* the red ejecta mass is really $\sim 0.04 M_\odot$ (but see our discussion below), then we would lack a convincing explanation of the red kilonova, since tidal ejecta are challenged to produce the needed large amount of

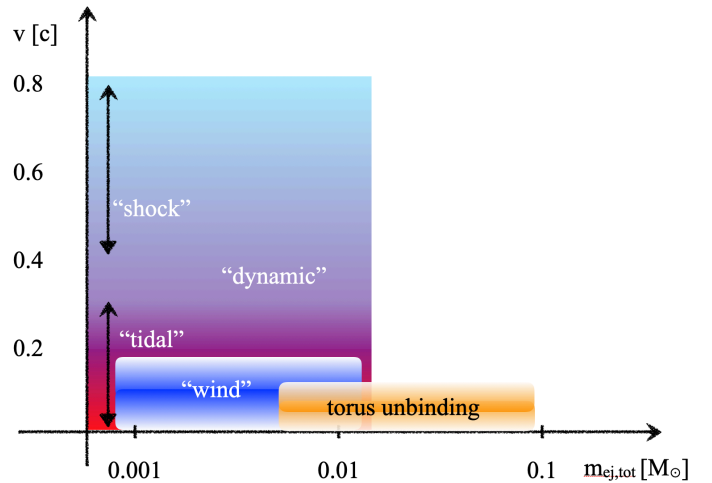


Figure 4: Sketch of the total masses and expected velocity ranges in different ejecta channels.

mass.⁵

We sketch in Fig. 4 the currently expected ranges of total ejecta mass and velocity.

2.3 Radioactively powered transients

Partially sparked by a conference proceedings article showing the first nucleosynthesis calculations for neutron star merger ejecta,^[46] Li & Paczyński^[145] explored in a simple model what a neutron star merger’s electromagnetic emission due to radioactive ejecta may look like. They realized that due to the small ejecta mass and the rapid expansion velocity a short-lived supernova-like transient should result. As in a thermonuclear supernova, the bulk of the initial internal energy is consumed in the optically thick, initial expansion phase and detectable emission can only be expected, if at the time when $t = \tau_{\text{diff}}$, the latter being the diffusion time, a (radioactive) heating source is present. Adopting an effective gray opacity of $\kappa = 0.2 \text{ cm}^2 \text{ g}^{-1}$, Li & Paczyński predicted a one-day lasting blue transient with a peak luminosity of over $10^{44} \text{ erg s}^{-1}$. Metzger et al. in Ref. [146] improved on this simple model by using nuclear network calculations to determine the nuclear heating rate and by applying 1D radiative transfer to calculate light curves. Using (the too low) gray opacity representative for iron group elements, they found transients peaking after ~ 1 day in the optical, but with luminosities that are more than two orders of magnitude lower than found by Li & Paczyński.^[145]

Soon after, it was realized^[147,148] that ejecta consisting of r -process elements, in particular if they include lanthanides and actinides, contain orders of magnitude more optical transition lines than the iron-group elements. In an expanding medium, such as merger ejecta, these lines dominate the material opacity, raising it by a factor of ~ 10 for the light r -process, and a factor of 100 to 1000 for lanthanides and actinides.^[147–149] Thus, if heavy r -process is present, one ex-

⁵Some extreme models with both an extreme mass ratio of $q \approx 0.5$ and the extremely stiff MS1b EOS could produce such large ejecta masses.^[94] The MS1b EOS, however, is strongly disfavoured by the LVC results on the tidal deformability in GW170817.^[144]

pects a more modest peak luminosity of $\sim 10^{41}$ erg s $^{-1}$ and a transient duration of about a week. Soon after these new insights on the opacity, it became clear that the various ejecta of neutron star mergers contain a broad range of electron fractions^[71–73] so that both a “red” and a “blue kilonova” are plausible possibilities.

The calculations of Ref. [147, 148] predicted broad spectral features, but no individual lines due to large expansion velocities. Of all the lanthanides and actinides, neodymium is expected to dominate the opacity.^[150–152] Early spectra appear as an almost featureless blue continuum blackbody that rapidly shifts to longer wavelengths, peaking in near-infrared on a timescale of a week.^[153] Later spectra strongly deviate from blackbody, showing broad spectral features and a sharp cutoff at shorter wavelength.^[153, 154]

Effects from matter not being in local thermodynamic equilibrium (“NLTE effects”) are expected for both early and late spectrum individual lines, so a correct prediction of spectra requires NLTE effects to be accounted for.^[155, 156] A detailed analysis of the cooling mechanisms shows that the temperature is supposed to remain approximately constant for an extended period of time, providing an unchanged spectrum for several weeks.^[156, 157] NLTE effects in kilonova are only being tackled now and they are currently an area of active research.

3 Confronting observations

While the above outlined picture has, despite its shortcomings, a sound physical basis, only some of the described aspects are observationally confirmed. What *are* the observational facts that we can consider as firmly established? We will review them here as a guidance to understand where our theoretical picture needs to be refined further in future work. What we discuss here is certainly biased by our incomplete knowledge of the rapidly growing literature on the topic.

The visible and IR emission that followed the first observed neutron star merger GW170817 showed an early blue emission in the first 2–3 days, followed by a longer-lived red transient that decayed on a time scale of about a week.^[124–126, 158–160] While rapidly rising initial blue emission is inconsistent with high-opacity “main” r -process (including lanthanides and heavier nuclei), blue emission is exactly what is expected from radioactively powered light r -process ejecta.^[122] The relatively large “blue” ejecta masses and velocities ($\sim 0.025 M_{\odot}$ and $\sim 0.3c$, see Ref. [150]), however, are larger than what is expected from neutrino-driven winds alone. They could be accommodated, e.g. by the above discussed spiral-wave winds, provided that the central remnant survives for a few hundred milliseconds. One possible explanation for the high expansion velocity of the blue component is that we are actually observing fast-moving dynamical ejecta, which is reprocessing the flux from deeper, slower-moving layers.^[161] Light r -process elements, however, are not the only possible explanation, other suggestions for the origin of the blue component include cocoon shock cooling,^[162] or magnetar-like central engine activity.^[127, 163]

A longer lasting, redder component, on the other hand, is consistent with high-opacity, lanthanides-rich ejecta.^[150, 160, 164] The overall observed energetics, i.e. the bolometric lumi-

osity, of AT2017gfo fits very well with the nuclear heating due to decaying r -process elements.^[69, 165] While we consider this as strong evidence for the production of r -process elements, it is not particularly constraining in terms of which elements are involved, since a broad range of electron fractions, $Y_e \sim 0.05 - 0.35$, produces nearly the same, power-law like heating (see Appendix A).

The exact composition is more difficult to infer. Spectral calculations were used to interpret features in the spectrum of AT2017gfo as being due to the presence of strontium, a light r -process element from the first r -process peak.^[166–168] The presence of Sr would imply that the blue component of the ejecta were rather proton-rich, with $Y_e > 0.4$,^[167] while at the same time the bolometric luminosity suggests that the bulk of the ejecta should have $Y_e \leq 0.35$.^[69] Given that the pre-merger neutron stars contain only a very small mass fraction with $Y_e > 0.1$ ($\sim 10^{-4}$; see Fig. 23 in Ref. [41]), this also underlines the pivotal role that weak interactions play in a neutron star merger.

While the presence of Sr is plausible, its unique identification is a very challenging task and the so far collected evidence cannot be considered as conclusive⁶. The challenges arise on the one hand from a serious lack of relevant and reliable atomic data, in particular for elements in the second r -process peak.^[169] On the other hand, existing studies have a large number of free parameters out of which some are fixed “by hand” to plausible values while others are varied to obtain agreement between simple models and observations. This raises, of course, questions about the uniqueness, robustness, and consistency of the results⁷. Helium has been considered as an alternative explanation for a spectral feature at 8000 Å, but no conclusive evidence was found.^[170] A search for some of the third r -process peak elements such as Pt and Au in the photosphere was performed,^[168] but with negative results.

The week-long red transient, however, is not the only evidence for the lanthanide-rich ejecta. Other indications include the temperature plateau at 2500 K after > 5 days,^[171] near-infrared spectral features^[158, 159, 172, 173] and the late-time bolometric light curve.^[69, 165, 174] Finally, there are new indications of features of doubly-ionized La and Ce in the early spectrum of AT2017gfo.^[175] It is worth noting that the early blue emission was detected with broad spectral features indicating rapid photospheric expansion with the velocities $> 0.3 c$.^[158, 176] At the same time, the redder, lanthanide-rich component had more narrow features, consistent with lower expansion velocities. Interpreting the data on the basis of 1D spherically-symmetric models, one finds the lanthanide-rich ejecta to be relatively massive ($> 0.04 M_{\odot}$) and slow ($\sim 0.1 c$).^[129, 171, 177, 178] Models that incorporate asphericity, however, allow to explain the same signal with smaller masses of lanthanide-rich ejecta^[128, 153, 161] and faster expansion. The presence of lanthanide features in the early emission is consistent with small amounts of rapidly expanding dynamical ejecta.^[161] There is no consensus yet about the number of

⁶We are grateful to Eli Waxman for sharing his detailed viewpoints on this topic with us.

⁷For example, Ref. [169] find best-fit density values that are substantially below those found in the hydrodynamic simulations they use to determine abundances. Such low values may actually be challenged to reproduce the minimum mass that is needed to explain the bolometric luminosity of AT2017gfo, $m_{\text{ej}} > 0.015 M_{\odot}$.^[69]

ejecta components, some argue that models need to include at least three ejecta components,^[129,177] while others argue that even a single composition component can explain the basic properties.^[179]

In the mid-IR spectrum of AT2017gfo, observations with Spitzer telescope showed strong emission at 43 days after the NS merger event GW170817 at $4.5 \mu\text{m}$, but nothing at $3.6 \mu\text{m}$.^[174] This could indicate the existence of a strong spectral line around this region, which could be explained with an emission by W or Se ions.^[180] Features from late-time Spitzer observations are consistent with being produced by the decay of the heaviest isotopes with a half-life around ~ 14 days (e.g. ^{225}Ra),^[172,173] but could potentially also be explained by a composition with only light r -process elements.^[181]

Another important class of observational constraints on the r -process production comes from metal-poor galactic halo stars. It has long been established that the so-called “universal r -process” spanning the region between Ba and Ir in metal-poor stars and in solar r -process residuals is essentially identical, within the measurement uncertainty.^[40,74] This means that the primary r -process site responsible for the majority of the heavy r -process, must do it in a manner which respects this observational pattern. If mergers are responsible for the r -process, this excludes certain channels such as, for example, winds from a hypermassive merger remnant, or shock dynamic ejecta, where electron fraction is raised and the r -process pattern becomes strongly sensitive to the hydrodynamics conditions.

We do not have accurate measurements of the r -process in GW170817, but we can compare the estimated fraction of the lanthanides to what is observed in r -enhanced halo stars. Assuming that neutron star mergers are responsible for the majority of the r -process, the estimates of the lanthanide fraction synthesized in such a merger yield $\log X_{\text{La}} \sim -2 \pm 0.5$ dex, while for the r -enhanced halo stars this fraction is significantly higher: $\log X_{\text{La}} \sim -1.5$ dex.^[182] The general consensus about kilonova GW170817 is that the total fraction of synthesized lanthanides should be $\log X_{\text{La}} = -2.2 \pm 0.5$, which is therefore in tension with the r -enhanced halo stars.^[182] This may mean that GW170817 was not a typical merger event, and lanthanides were underproduced. Another possible way to resolve this discrepancy is the directional dependence in the neutron-to-proton ratio in the ejecta, which may not necessarily mix very well in the galactic halo. It is also possible that the range of X_{La} produced in neutron-star mergers is broader, or that another source was contributing to the r -process at low metallicities. As a result, different halo stars may have been enriched by different parts of the ejecta from a single merger. This is an additional factor increasing variability in the observed lanthanide fraction within the population of halo stars.

In Fig. 5 we provide an update of our Fig. 2 from Ref. [31]. If we take the solar-system r -process pattern^[183] as representative, assume a baryonic mass of the Milky Way of $6 \times 10^{11} M_{\odot}$ and assume $\approx 10^{10}$ yrs for the age of the Galaxy, we find a rough r -process production rate of $\approx 1.6 \times 10^{-6} M_{\odot} \text{ yr}^{-1}$ for all r -process and $\approx 2.5 \times 10^{-7} M_{\odot} \text{ yr}^{-1}$ as production rate for the r -process elements heavier than $A > 130$. These production rates must be the product of the average event rate and the average ejecta mass (in the considered A -range). For

a given average event rate density (on the x-axis; in events per Myr^{-1} and “Milky Way equivalent Galaxy” (MWEG)^[184] on the bottom and in events per year and Gpc^{-3} on the top), the average ejecta mass required to produce all of the Galactic r -process is shown as the black solid line from the upper left to lower right. The corresponding lines for heavy ($A > 130$) and light r -process ($80 < A \leq 130$) are shown as solid red and dashed blue lines, respectively. The estimated neutron star merger and neutron star black hole merger event rates from the LIGO/Virgo collaboration^[185] are also shown as well as short GRB rates^[186] and rate estimates based on Galactic pulsar binaries.^[187] In addition, we overplot ejecta masses from various simulation. As an example, if the average neutron star merger rate were $2 \times 10^{-5} \text{ yr}^{-1} \text{ MWEG}^{-1}$, a merger would need to eject about $10^{-2} M_{\odot}$ of heavy r -process event in order to account for the heavy r -content in the Galaxy.

4 Directions for the future

As outlined above, a lot of theoretical groundwork has been laid in the last two decades with a major confirmation of the overall big picture (and a lot of inspiration) coming from the first detected neutron star merger GW170817/AT2017gfo. However, many aspects have so far remained un- or at least insufficiently explored. We give here a brief overview of possible future directions and for some of these explorations the nuclear heating library described in Appendix A may be useful.

The r -process site has remained a mystery for so many decades, because it involves major challenges on both the nuclear and the astrophysical side. On the nuclear physics side, properties of extremely neutron-rich nuclei (close to the neutron drip line) are needed which include nuclear masses, β -decay half-lives, neutron capture and fission rates. On the astrophysical side, all of the promising production sites involve extremely strong gravitational and likely magnetic fields and densities and temperatures far beyond anything else that exists in the post-Big Bang Universe. In what follows below, we focus on the astrophysical side, for a discussion of the involved nuclear physics we refer the interested reader to the excellent recent review of Ref. [40].

4.1 The scale challenge

For GW170817, gravitational waves and, much later, a firework of electromagnetic emission, including a kilonova, was observed. The gravitational waves are shaped by matter at supra-nuclear densities, moving at a substantial fraction of the speed of light in a strongly curved, dynamical spacetime. Close to merger, the typical time scales are \sim milliseconds, and the typical length scales ~ 10 km. After the merger, in most cases, a close-to-collapse, neutron star-like object with densities close to $\sim 10^{15} \text{ g cm}^{-3}$ and temperatures substantially exceeding 10^{11} K ^[190] forms, which emits kHz gravitational waves and radiates neutrinos at luminosities exceeding the solar luminosity by a whopping factor of $\sim 10^{20}$.

The kilonova emission, in contrast, peaks at time scales of ~ 1 week, when the ejecta have expanded to $\sim 10^{10}$ km, and the densities have dropped to $\sim 10^{-14} \text{ g cm}^{-3}$ (see, e.g. Fig. 1 in Ref. [191]). The physics that determines this stage is

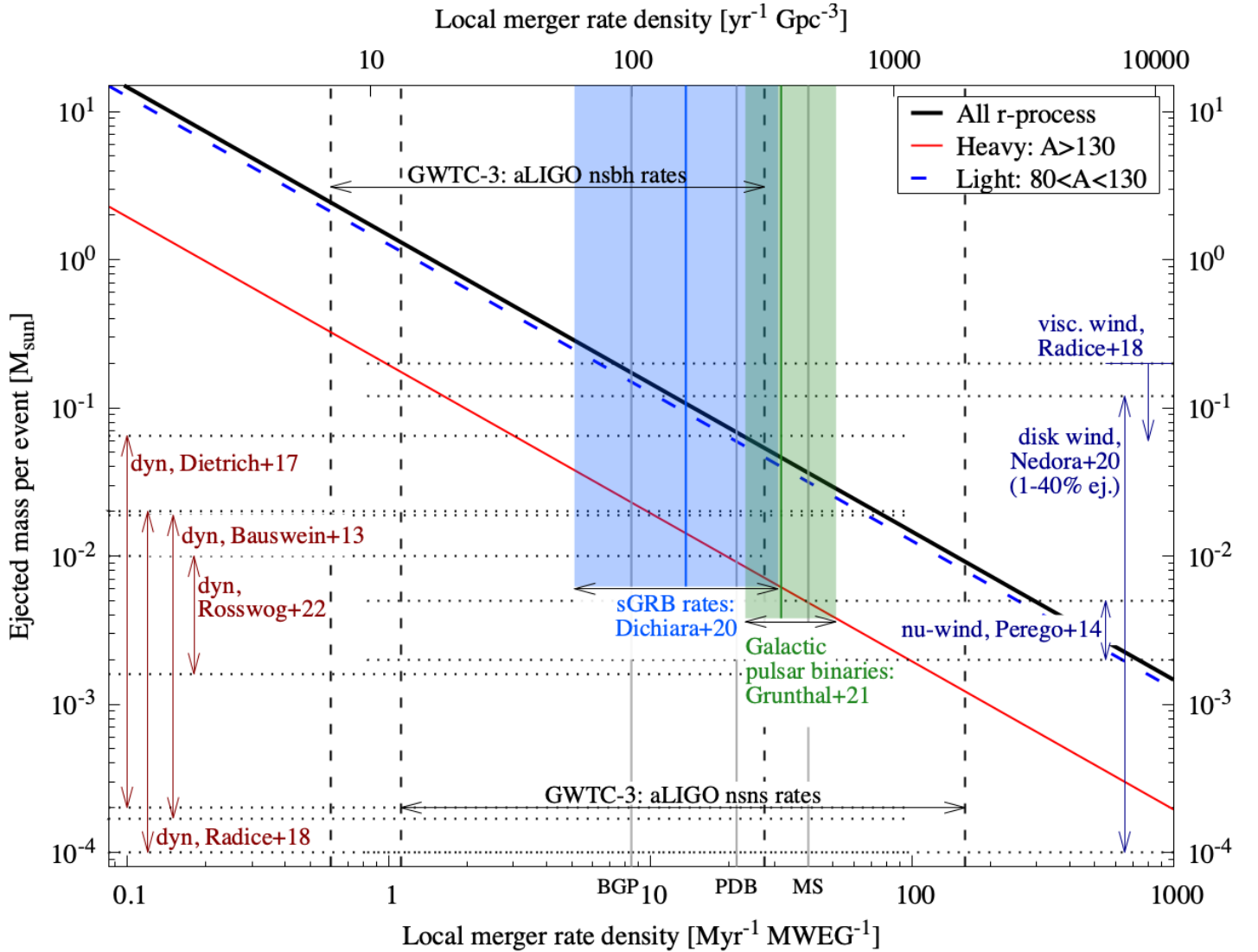


Figure 5: The figure shows how much r -process needs to be ejected per event (diagonal lines from upper left to lower right) to explain the observed r -process material (update of Fig.2 from Ref. [31]). In addition, various rate estimates and ejecta masses from simulations are shown.

The horizontal axis shows the local merger rate density using different units on the top and bottom axes. The units on the top axis are events per year in Gpc^3 , while the units on the bottom are events per million years, per Milky Way Equivalent Galaxy (MWEG). We use the conversion factor of $1 \text{ Myr}^{-1} \text{ MWEG}^{-1} = 11.7 \text{ yr}^{-1} \text{ Gpc}^{-3}$, corresponding to 1.17×10^7 MWEGs in Gpc^3 .^[188,189] The vertical axis shows the ranges of ejecta masses produced via different ejection channels, or, respectively, needed to produce ranges of observed r -process material (top-left to bottom-right lines). Also shown are various rate estimates, including LVC estimates for nsns and nsbh binaries as well as rates based on short GRBs^[186] and Galactic pulsar binaries.^[187] The labels BGP, PDB and MS on the horizontal axis refer to different statistical models used to process the data in Gravitational Wave Transient Catalog 3 (GWTC-3) in Ref. [185]: BGP refers to “binned Gaussian processes”, PDB refers to “power law + dip + break”, and MS refers to the “power law + peak multi-source” model of Ref. [185]. The grey solid vertical lines indicate the expectation values of these models. Ranges of masses of dynamical ejecta, indicated on the left, are taken from Ref. [52,92–94]. Disk wind mass range on the right is computed by taking 1 – 40 % of the torus mass calculated in Ref. [70]. Neutrino-driven wind mass estimate is taken from Ref. [55], while upper limit on the mass of viscously ejected wind is from Ref. [65].

the heating by radioactive decays, the thermalization of the decay products, atomic line opacities and, at late stages, NLTE effects in the rapidly expanding gas cloud. So between the observed signatures, gravitational waves and kilonova, there is a huge gap in scales, physics and observations and also in our understanding of what is actually happening. This gap is so far usually bridged by making strongly simplifying assumptions such as homology and/or spherical symmetry, but the real picture is likely substantially more complicated, for example geometric effects, nuclear heating etc. can still impact the evolution significantly.^[128, 191, 192] In other words, there is plenty of room for interesting new explorations.

4.2 3D geometry of ejecta components

4.2.1 Different ejection channels and their possible interactions

The “easiest” to handle ejection channel are dynamical ejecta that are purely hydrodynamically launched. But even this, “easy”, task requires at least 3D full GR hydrodynamic simulations of tens of ms that include a temperature-dependent, nuclear equation of state and a reliable treatment of weak interactions/neutrinos. Other effects such as magnetic fields and/or viscous dissipation can likely be ignored in these early stages, but will become important later. Wind ejecta simulations need to be run for substantially longer time scales (~ 100 ms), and, due to the longer time scales, need a fairly accurate neutrino transport and should ideally also include the evolution of the magnetic field. The same physics ingredients, but even longer time scales ($\sim 1 - 10$ s) are needed for the torus unbinding. In 3D, this can to date only be done for black hole torus systems, where the spacetime can be considered as stationary (i.e. Kerr) and the numerical time step is set by the sound speed in the torus^[193, 194] (rather than by the speed of light). While current explorations starting from (non-selfgravitating) equilibrium tori around Kerr black holes are important steps for sharpening our understanding, it remains to be seen how realistic they really are, given that the tori formed in violent mergers of neutron stars and black holes are likely very far from being in equilibrium. For a central neutron star, the space-time has to be dynamically evolved which substantially increases the computational costs. To date, this challenge can only be met with 2D simulations.^[195]

An interesting, but so far hardly explored question is the interaction between different ejecta components. This could emerge, for example, if tidal dynamical ejecta are launched first, but faster “shock” ejecta produced by quasi-radial oscillations of the central remnant catch up with them.^[105] If occurring close enough, the resulting shock could produce large enough temperatures to raise the electron fraction, otherwise at least a mixing between higher- and low- Y_e material would occur. This could lead to electron fraction distributions that are far more complicated than what is usually assumed in kilonova models.

Another interesting interaction could occur between matter that is nearly unbound, but falls back after some time towards the central source. This matter could interact with and potentially bury late-time disk ejecta.

Virtually guaranteed interactions, of course, come from the relativistic, jetted outflows that are needed to produce

GRBs.^[196–199] They are usually assumed to go along with black hole formation, but a recent study^[200] finds that they could also emerge with a central neutron star being present⁸. The interaction of jets with the other ejecta components may substantially impact the electromagnetic emission and detectability.^[165, 202–210] For example, the neutrino-driven wind simulations of Ref. [55] show low Y_e material at the leading edge of the wind ejecta which “shield” inner, higher Y_e ejecta. Even very small ($\gtrsim 10^{-4}$) mass fractions of lanthanides or actinides can be very effective in obscuring a blue kilonova component seen behind an ejecta component which contains lanthanides. The latter acts as a “curtain” that efficiently occludes the visible light emitted at deeper layers.^[211, 212] A jet plowing through these wind ejecta would punch a “hole” into this lanthanide curtain thus allowing bluer radiation to escape from the polar region.^[208]

4.2.2 Multidimensional radiative transfer effects

Several studies have begun to explore multi-dimensional effects in the kilonova signals^[128, 153, 161, 191, 213] and found that they can have a significant influence, controlling an order of magnitude of the apparent kilonova luminosity. This is dramatically different from the initial estimates, which argued that the directional variability can be reduced to the projected area of the photosphere along the line of sight, and therefore should only affect kilonova luminosity within about a factor of two.^[214, 215] While this may be a result of the used gray-opacity approximation, more advanced radiative transfer simulations with detailed, density-dependent opacities, reveal strong density-driven effects on light curves and spectra.^[128] It will be up to numerical simulations to clarify which range of density profiles is actually realized in the different ejection channels or by their interaction.

Many numerical simulations predict aspherical, approximately axisymmetric shapes of the ejecta, with a gradual change in the neutron-to-proton ratio as a function of the polar angle. In the emerging picture that the “red” lanthanide-rich ejecta have approximately toroidal shape, while the polar regions are occupied by lighter r -process, “blue” ejecta. But for mass ratios q deviating substantially from unity, the tidal ejecta can form spiral arms that break axisymmetry, under certain conditions dynamical ejecta can produce “lanthanide pockets”^[105] and long-term simulations of post-merger disks show radially dependent composition profiles that are relics of the accretion history.^[216] Such effects are usually neglected in kilonova model explorations (with some notable exceptions^[217]). On the other hand, the dynamic ejecta that result from shocks possess sufficiently high entropy to form an almost-spherical remnant after its expansion to homology.^[93]

Another way in which the shape of the ejecta can play a tremendous role is via the above described “lanthanide curtaining”. This “lanthanide curtaining” could manifest itself as an “opening angle” around the kilonova pole, being the maximum angle at which the blue emission is still visible. Perhaps in the future, two categories of kilonovae will be identified: some with rapidly-rising, short-lived blue transients, and others without, where “lanthanide curtaining” is operating.

⁸The basic picture of highly magnetized neutron star-like objects producing GRBs had been outlined already earlier, see Ref. [201]

In a multi-component, multi-dimensional setting, several other effects can manifest themselves and must be considered when interpreting kilonovae signals, such as e.g. flux reprocessing,^[161] or the orientation dependence of the width of the spectral features such as P Cygni features.^[128] Higher expansion velocities across the line of sight smear out even broad features and present significant stumbling blocks for identifying elements.

The shape of the ejecta right after their launch by the central engine can differ significantly from their shape at the kilonova epoch.^[191] The r -process occurring in the ejecta lasts for about one second and can generate a sizeable fraction of the total kinetic energy of expansion and thus modify the distribution of ejecta mass in the velocity space. The peak nuclear energy injection happens at around one second, and depends on the expansion velocity and in particular the neutron richness (see Appendix A). On the second and subsequent timescales, variations in the nucleosynthesis in neighboring parcels of expanding fluid can create fluid motions and possibly internal shocks. More work needs to be done to understand the extent of this reshaping and related possibilities of internal shocks due to inhomogeneities in nuclear heating. The nuclear heating library that is provided with this study covers the range of timescales where the ejecta reshaping is happening, and could help understanding such effects.

Much later, at the kilonova epoch, the ejecta is in the state of free homologous expansion, when different fluid parcels are out of sonic contact with each other and the changes in its morphology are completely negligible.

4.3 NLTE effects and spectra at late times

At the time of writing, despite considerable efforts, no simulated spectra have been produced for the late-time epoch (> 7 days) that match AT2017gfo well enough to deduce the presence, let alone abundances, of individual elements (evidence for the element Sr in early spectra is still inconclusive). In particular, the anomalously bright visible bands at late epoch are in tension with all current models that use detailed opacities.^[160]

It is highly likely that the assumption of local thermodynamic equilibrium (LTE), employed in opacity calculations and in radiative transfer simulations, is the one to blame for these discrepancies between theory and observation. Relaxing this assumption to produce so-called “NLTE” simulations of opacity and radiative transfer, is not possible at present time. All currently used radiative transfer models use the assumption of LTE, which means that the populations of ionized and excited states are calculated using a single temperature, by solving the Saha-Boltzmann equation. Fully removing the assumption of LTE in atomic population calculations is a daunting computational task for the heavy elements produced in the r -process, due to the colossal number of atomic energy levels involved, and the need to invert a matrix with the rank equal to the number of those levels, associated with a system of coupled rate equations.^[154]

In spite of these difficulties, work has been started on the nebular phase of kilonovae, where NLTE effects play the dominant role.^[155–157] Elements Se ($Z = 34$) and W ($Z = 74$) have been implicated in producing a peculiar line feature at

4.5 μm at the nebular phase.^[180]

Estimates of the rates of kinetic processes in the nebular phase indicate that the so-called coronal approximation is applicable at late epochs.^[156] Because the ejecta do not have a photosphere in nebular phase, its cooling is no longer efficient, and the rates of individual kinetic processes must be considered. In the coronal approximation, the radiative field is considered negligible in determining the excitation and ionization structure, and therefore the material emissivity can be considered as only dependent on the plasma density and effective electron temperature. Moreover, electronic excitations and ionizations are dominated by collisions with fast electron populations generated by radioactivity, rather than by collisions with thermal Maxwellian electrons that are strongly subdominant. The energy budget in the electron population is balanced by the influx of new high-energy β -particles produced by radioactivity, and by inefficient NLTE cooling via collisions with ions. The NLTE spectrum directly reflects the β -radioactivity in the ejecta, so the nebular emission can be thought of as an r -process radioactivity, cascaded down to the visible and infrared range. Simulating realistic spectra in such regime may require not only a NLTE treatment, but also detailed electron transport models which go beyond the single kinetic temperature.^[155]

4.4 Electron thermalization

Thermalization of high-energy decay radiation directly affects the luminosity of a kilonova. Unlike supernovae where γ -radiation is the dominant source of heating, the r -process powered kilonovae are heated predominantly by β -particles. While under certain conditions of neutron richness, specific nuclear mass models predict that fission products dominate the nuclear heating,^[218] for example in the case of the fission of ^{254}Cf , in the majority of interesting cases the nuclear heating on kilonova time scales is due to the energy released in β -decays.^[219] A few simple, but powerful prescriptions were derived for the thermalization efficiency.^[220, 221] These prescriptions, however, assume a rather simple homogeneous background. As explained above, a population of such fast electrons determines the nebular emission.^[157] Current challenges include the modeling of populations of such high-energy electrons. The latter depends on the nuclear physics and, in addition, on the state of the involved magnetic fields. If magnetic fields in neutron stars are on the order of 10^{12} G, then conservation of magnetic flux confines the electrons to Larmor radii that are about 10^{-4} of the ejecta radius at 100 d.^[155, 220, 222] A comprehensive code with full electron transport is required to better understand the thermalization process.

In the future, full electron transport codes will be needed to validate the existing approximations and to explore the extent to which kilonovae are sensitive to it. In the provided heating library, roughly 25% of the energy can be considered to come from β -particles (with the rest of the energy being lost to γ -photons and neutrinos at late times). An average energy of a β -particle is $\sim 0.5 \pm 0.2$ MeV;^[220] these numbers, along with the heating rates, can be used as an input to electron transport codes for corresponding sensitivity studies.

5 Summary

One of the arguably most important consequences of a neutron star merger is that it ejects a fraction of its mass as neutron-rich matter into space. This matter experiences rapid neutron capture nucleosynthesis and the decay of the freshly synthesized, unstable nuclei powers a thermal, relatively isotropic electromagnetic transient. Such transients provide precious *additional* information that is not contained in the gravitational wave signal which delivers insights into both the extreme physics at work during a merger as well as into the astronomical environment where it occurs.

Just a few months prior to the start of the fourth LIGO-Virgo-KAGRA observation run (“O4”), we summarized here our current understanding of the various ejection channels, the expected ejecta properties and how this translates into potentially observable thermonuclear transients. We also stated important issues where no agreement has been reached yet and we discussed possible ways forward, into so far unexplored scientific territory. And we hope, of course, that soon more light will be shed on this exciting topic by future multi-messenger observations.

Acknowledgements

SR would like to thank Eli Waxman for the invitation to a very inspiring workshop on the GW-EM connection at the Weizmann Institute. Thanks also to all the participants for creating a constructive brainstorming atmosphere. OK is grateful to Ryan T. Wollaeger, Jonah M. Miller and Chris L. Fryer for helpful comments and spirited discussions. We are further grateful to Jonah Miller, Udi Nakar, Quantin Pognan, David Radice, Daniel Siegel and the two anonymous referees for their careful reading of a first version of this manuscript and for their insightful comments.

SR has been supported by the Swedish Research Council (VR) under grant number 2020-05044, by the research environment grant “Gravitational Radiation and Electromagnetic Astrophysical Transients” (GREAT) funded by the Swedish Research Council (VR) under Dnr 2016-06012, by the Knut and Alice Wallenberg Foundation under grant Dnr. KAW 2019.0112, by the Deutsche Forschungsgemeinschaft (DFG, German Research Foundation) under Germany’s Excellence Strategy -EXC 2121- ”Quantum Universe” - 390833306 and by the European Research Council (ERC) Advanced Grant INSPIRATION under the European Union’s Horizon 2020 research and innovation programme (Grant agreement No. 101053985). SR’s calculations were performed on the facilities of the North-German Supercomputing Alliance (HLRN), on the resources provided by the Swedish National Infrastructure for Computing (SNIC) in Linköping, partially funded by the Swedish Research Council through Grant Agreement no. 2016-07213, and at the SUNRISE HPC facility supported by the Technical Division at the Department of Physics, Stockholm University. Special thanks go to Holger Motzkau and Mikica Kocic for their excellent support in upgrading and maintaining SUNRISE. This work was supported by the US Department of Energy through the Los Alamos National Laboratory. Los Alamos National Laboratory is operated by Triad National Security, LLC, for the National Nuclear Secu-

rity Administration of U.S. Department of Energy (Contract No. 89233218-CNA000001). Research presented in this article was supported by the Laboratory Directed Research and Development program of Los Alamos National Laboratory under project number 20200145ER. All LANL calculations were performed on LANL Institutional Computing resources.

Conflict of Interest

The authors declare no conflict of interest. Approved for public release with designated number LA-UR-22-25522; distribution is unlimited.

A Appendix: Publicly available nuclear heating information

Here we provide a concise description of a publicly available heating rate library that is based on the Winnet network.^[223, 224] Winnet itself is based on the BasNet network^[225] and it contains 5831 isotopes between the valley of stability and the neutron drip line, starting with nucleons and reaching up to $Z = 111$. The implemented reaction rates are from the compilation of Ref. [226] and based on the Finite Range Droplet Model (FRDM).^[227] The electron-/positron capture and β -decay rates are taken from Ref. [228] and Ref. [229], the neutron capture and neutron-induced fission rates are due to Ref. [230] and the β -delayed fission probabilities from Ref. [231] are implemented. Below, we provide a library of heating rates as direct output from Winnet and we further provide a simple fit formula which may be more convenient for the implementation of nuclear heating into hydrodynamic simulations.

Heating library

We produced a heating rate library that is based on parametrized trajectories that cover a broad range of conditions relevant for neutron star merger ejecta. The setup of the trajectories is the same as described in Sec. 2.2 and 2.3 of our earlier work.^[31] For the mass that is used to set up the initial trajectory, we adopt $m_{\text{ej}} = 0.05 M_{\odot}$, close to the estimate for GW170817.^[69, 124, 129, 150, 160, 165, 177] The energy output is in units of $\text{erg}/(\text{g s})$ (i.e. independent of the ejecta mass) and our value for m_{ej} only impacts the starting point of the trajectory, to which the heating rate is hardly sensitive. Another quantity that enters the calculation of the trajectory is the initial entropy s_0 . The nucleosynthesis (and therefore heating rate) at low values of Y_e is hardly impacted by the initial entropy,^[232] therefore, for tidal ejecta the heating rate is insensitive to the chosen entropy value. For neutrino-driven winds the entropy distribution is strongly peaked at $s \approx 15 k_{\text{B}}/\text{nucleon}$ ^[55, 72, 233] and we therefore choose this value for s_0 to determine the trajectory. Within the heating rate library, we vary the electron fraction Y_e between 0.05 and 0.5 in steps of $\Delta Y_e = 0.05$ and we explore velocity values of $[0.05c, 0.10c, 0.2c, 0.3c, 0.4c, 0.5c]$.

The corresponding heating histories, time in days and “naked” heating rate $d\epsilon/dt$ in $\text{erg}/(\text{g s})$ (i.e. no heating efficiency ap-

plied) and the resulting abundances can be downloaded at <http://compact-merger.astro.su.se/downloads.html>.

Fit formula

The following 13-parameter expression provides an acceptable (within 2%) fit for the simulated heating rates:

$$\frac{d\varepsilon}{dt} = \dot{\varepsilon}_0 \left(\frac{1}{2} - \frac{1}{\pi} \arctan \left[\frac{t - t_0}{\sigma} \right] \right)^\alpha \left(\frac{1}{2} + \frac{1}{\pi} \arctan \left[\frac{t - t_1}{\sigma_1} \right] \right)^{\alpha_1} + C_1 e^{-t/\tau_1} + C_2 e^{-t/\tau_2} + C_3 e^{-t/\tau_3} \quad (2)$$

Here, the first term in parentheses models a constant heating rate with a break to a power-law decay at t_0 , with a power-law index α and a transition width σ . The next term models a subsecond dynamics of the heating rate by a power-law raise with an index α_1 , threshold t_1 and a transition width σ_1 . The last two terms are needed to model the cases when individual isotopes dominate the power-law decay heating rates.

What we have just described is the raw nuclear energy generation rate. To obtain the energy input into the macronova/kilonova, some prescription for the thermalization efficiency needs to be applied, see e.g. Ref. [221].

References

- [1] A. G. W. Cameron, *Chalk River Rept.* **1957**, CRL-41.
- [2] E. M. Burbidge, G. R. Burbidge, W. A. Fowler, F. Hoyle, *Reviews of Modern Physics* **1957**, 29 547.
- [3] S. E. Woosley, J. R. Wilson, G. J. Mathews, R. D. Hoffman, B. S. Meyer, *ApJ* **1994**, 433 229.
- [4] K. Takahashi, J. Witt, H.-T. Janka, *A&A* **1994**, 286 857.
- [5] R. D. Hoffman, S. E. Woosley, Y.-Z. Qian, *ApJ* **1997**, 482 951.
- [6] K. Farouqi, K.-L. Kratz, B. Pfeiffer, T. Rauscher, F.-K. Thielemann, J. W. Truran, *ApJ* **2010**, 712 1359.
- [7] A. Arcones, H.-T. Janka, L. Scheck, *A & A* **2007**, 467 1227.
- [8] L. F. Roberts, S. E. Woosley, R. D. Hoffman, *ApJ* **2010**, 722 954.
- [9] T. Fischer, S. C. Whitehouse, A. Mezzacappa, F.-K. Thielemann, M. Liebendörfer, *A & A* **2010**, 517 A80.
- [10] L. Hüdepohl, B. Müller, H.-T. Janka, A. Marek, G. G. Raffelt, *Physical Review Letters* **2010**, 104, 25 251101.
- [11] L. F. Roberts, S. Reddy, G. Shen, *Phys. Rev. C* **2012**, 86, 6 065803.
- [12] G. Martínez-Pinedo, T. Fischer, A. Lohs, L. Huther, *Physical Review Letters* **2012**, 109, 25 251104.
- [13] G. Martínez-Pinedo, T. Fischer, L. Huther, *Journal of Physics G Nuclear Physics* **2014**, 41, 4 044008.
- [14] J. M. LeBlanc, J. R. Wilson, *ApJ* **1970**, 161 541.
- [15] E. M. D. Symbalisty, D. N. Schramm, J. R. Wilson, *ApJ, (Letters)* **1985**, 291 L11.
- [16] A. G. W. Cameron, *ApJ* **2003**, 587, 1 327.
- [17] S. Nishimura, K. Kotake, M.-a. Hashimoto, S. Yamada, N. Nishimura, S. Fujimoto, K. Sato, *ApJ* **2006**, 642, 1 410.
- [18] P. Mösta, C. D. Ott, D. Radice, L. F. Roberts, E. Schnetter, R. Haas, *Nature* **2015**, 528, 7582 376.
- [19] N. Nishimura, H. Sawai, T. Takiwaki, S. Yamada, F. K. Thielemann, *ApJ, (Letters)* **2017**, 836, 2 L21.
- [20] P. Mösta, L. F. Roberts, G. Halevi, C. D. Ott, J. Lipuner, R. Haas, E. Schnetter, *ApJ* **2018**, 864, 2 171.
- [21] M. Reichert, M. Obergaulinger, M. Eichler, M. Á. Aloy, A. Arcones, *MNRAS* **2021**, 501, 4 5733.
- [22] J. Pruet, S. E. Woosley, R. D. Hoffman, *ApJ* **2003**, 586, 2 1254.
- [23] J. Pruet, T. A. Thompson, R. D. Hoffman, *ApJ* **2004**, 606, 2 1006.
- [24] R. Surman, G. C. McLaughlin, W. R. Hix, *ApJ* **2006**, 643 1057.
- [25] D. M. Siegel, J. Barnes, B. D. Metzger, *Nature* **2019**, 569, 7755 241.
- [26] D. M. Siegel, *European Physical Journal A* **2019**, 55, 11 203.
- [27] J. M. Miller, T. M. Sprouse, C. L. Fryer, B. R. Ryan, J. C. Dolence, M. R. Mumpower, R. Surman, *ApJ* **2020**, 902, 1 66.
- [28] R. Surman, G. C. McLaughlin, *ApJ* **2004**, 603, 2 611.
- [29] D. M. Siegel, B. D. Metzger, *Physical Review Letters* **2017**, 119, 23 231102.
- [30] Y.-Z. Qian, *ApJL* **2000**, 534 L67.
- [31] S. Rosswog, U. Feindt, O. Korobkin, M.-R. Wu, J. Sollerman, A. Goobar, G. Martínez-Pinedo, *Classical and Quantum Gravity* **2017**, 34, 10 104001.
- [32] E. Nakar, *Phys. Rep.* **2020**, 886 1.
- [33] P. Beniamini, K. Hotokezaka, T. Piran, *ApJ* **2016**, 832 149.
- [34] A. P. Ji, A. Frebel, A. Chiti, J. D. Simon, *Nature* **2016**, 531, 7596 610.
- [35] T. T. Hansen, J. D. Simon, J. L. Marshall, T. S. Li, D. Carollo, D. L. DePoy, D. Q. Nagasawa, R. A. Bernstein, A. Drlica-Wagner, F. B. Abdalla, S. Allam, J. Annis, K. Bechtol, A. Benoit-Lévy, D. Brooks, E. Buckley-Geer, A. Carnero Rosell, M. Carrasco Kind,

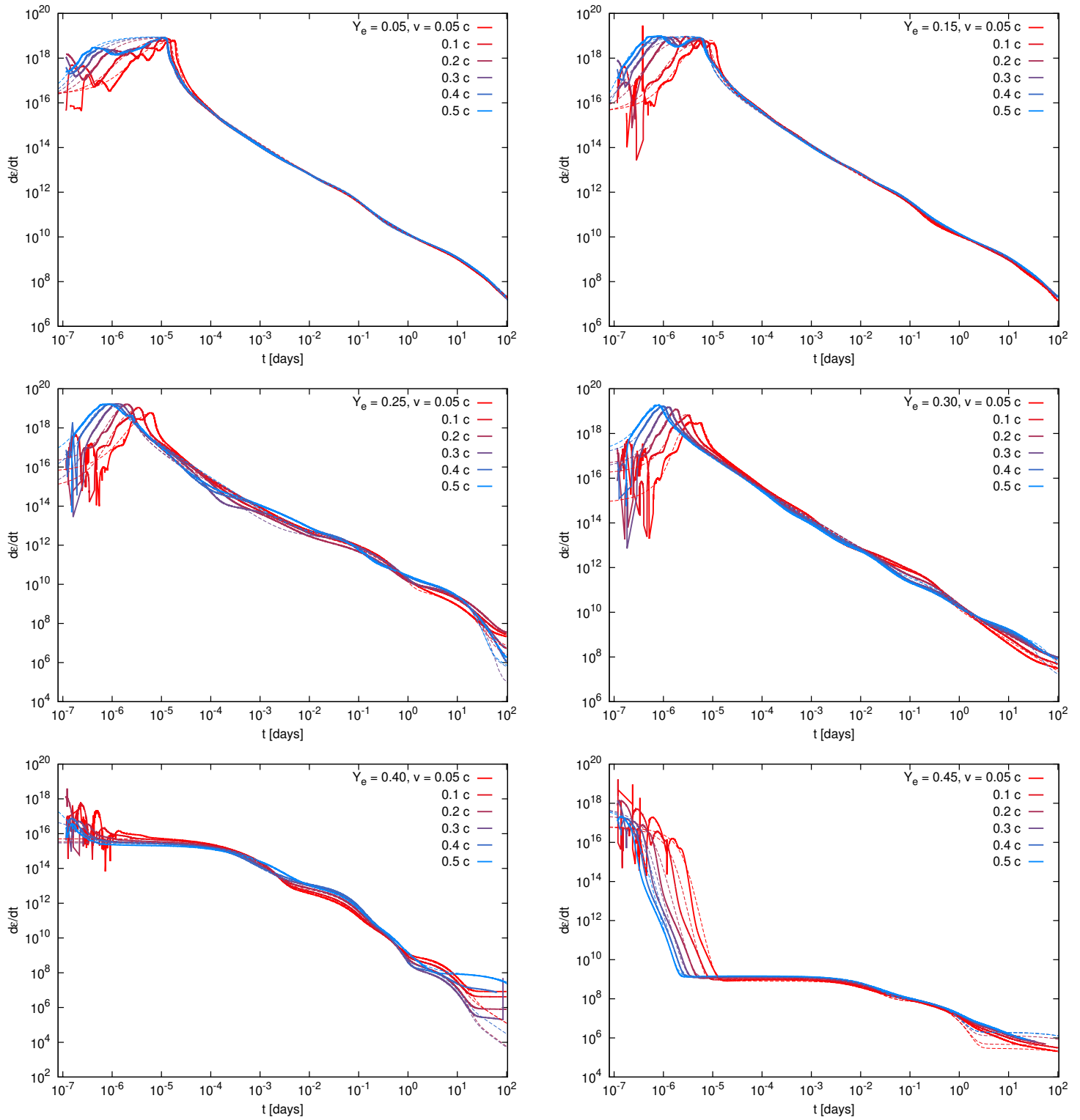


Figure 6: Example fits of the radioactive heating rate. Solid lines represent numerical rates computed with the nucleosynthesis network, and dashed lines are the fits.

Table 1: Fit coefficients

par. \ v_{ej}	Y_e	0.05c	0.1c	0.2c	0.3c	0.4c	0.5c	Y_e	0.05c	0.1c	0.2c	0.3c	0.4c	0.5c
$\dot{\epsilon}_0 \times 10^{18}$	0.05	10.0	10.0	10.0	10.0	10.0	10.0	0.1	10.0	10.0	11.0	11.0	11.0	11.0
α		1.37	1.38	1.41	1.41	1.41	1.41		1.41	1.38	1.37	1.37	1.37	1.37
t_0 (s)		1.80	1.40	1.20	1.20	1.20	1.20		1.40	1.00	0.85	0.85	0.85	0.85
σ (s)		0.08	0.08	0.095	0.095	0.095	0.095		0.10	0.08	0.07	0.07	0.07	0.07
α_1		7.50	7.50	7.50	7.50	7.50	7.50		9.00	9.00	7.50	7.50	7.00	7.00
t_1 (s)		0.040	0.025	0.014	0.010	0.008	0.006		0.040	0.035	0.020	0.012	0.010	0.008
σ_1 (s)		0.250	0.120	0.045	0.028	0.020	0.015		0.250	0.060	0.035	0.020	0.016	0.012
$\log C_1$		27.2	27.8	28.2	28.2	28.2	28.2		28.0	27.8	27.8	27.8	27.8	27.8
τ_1 (10^3 s)		4.07	4.07	4.07	4.07	4.07	4.07		4.07	4.07	4.07	4.07	4.07	4.07
$\log C_2$		21.5	21.5	22.1	22.1	22.1	22.1		22.3	21.5	21.5	21.8	21.8	21.8
τ_2 (10^5 s)		4.62	4.62	4.62	4.62	4.62	4.62		4.62	4.62	4.62	4.62	4.62	4.62
$\log C_3$		19.4	19.8	20.1	20.1	20.1	20.1		20.0	19.8	19.8	19.8	19.8	19.8
τ_3 (10^5 s)		18.2	18.2	18.2	18.2	18.2	18.2		18.2	18.2	18.2	18.2	18.2	18.2
$\dot{\epsilon}_0 \times 10^{18}$	0.15	14.0	10.0	11.0	11.0	11.0	11.0	0.2	14.0	10.0	10.0	10.0	11.0	11.0
α		1.41	1.38	1.37	1.37	1.37	1.37		1.36	1.25	1.32	1.32	1.34	1.34
t_0 (s)		1.00	0.80	0.65	0.65	0.61	0.61		0.85	0.60	0.45	0.45	0.45	0.45
σ (s)		0.07	0.08	0.070	0.065	0.070	0.070		0.040	0.030	0.05	0.05	0.05	0.050
α_1		8.00	8.00	7.50	7.50	7.00	7.00		8.00	8.00	7.50	7.50	7.00	7.00
t_1 (s)		0.080	0.040	0.020	0.012	0.012	0.009		0.080	0.040	0.030	0.018	0.012	0.009
σ_1 (s)		0.170	0.090	0.035	0.020	0.012	0.009		0.170	0.070	0.035	0.015	0.012	0.009
$\log C_1$		27.5	27.0	27.8	27.8	27.8	27.8		28.8	28.1	27.8	27.8	27.5	27.5
τ_1 (10^3 s)		4.07	4.07	4.07	4.07	4.07	4.07		4.07	4.07	4.07	4.07	4.07	4.07
$\log C_2$		22.0	21.5	21.5	22.0	21.8	21.8		23.5	22.5	22.1	22.0	22.2	22.2
τ_2 (10^5 s)		4.62	4.62	4.62	4.62	4.62	4.62		4.62	4.62	4.62	4.62	4.62	4.62
$\log C_3$		19.9	19.8	19.8	19.8	19.8	19.8		5.9	9.8	23.5	23.5	23.5	23.5
τ_3 (10^5 s)		18.2	18.2	18.2	18.2	18.2	18.2		18.2	18.2	0.62	0.62	0.62	0.62

- J. Carretero, C. E. Cunha, L. N. da Costa, S. Desai, T. F. Eifler, A. Fausti Neto, B. Flaugher, J. Frieman, J. García-Bellido, E. Gaztanaga, D. W. Gerdes, D. Gruen, R. A. Gruendl, J. Gschwend, G. Gutierrez, D. J. James, E. Krause, K. Kuehn, N. Kuropatkin, O. Lahav, R. Miquel, A. A. Plazas, A. K. Romer, E. Sanchez, B. Santiago, V. Scarpine, R. C. Smith, M. Soares-Santos, F. Sobreira, E. Suchyta, M. E. C. Swanson, G. Tarle, A. R. Walker, DES Collaboration, *ApJ* **2017**, 838 44.
- [36] T. Tsujimoto, T. Matsuno, W. Aoki, M. N. Ishigaki, T. Shigeyama, *ApJL* **2017**, 850, 1 L12.
- [37] A. Wallner, T. Faestermann, J. Feige, C. Feldstein, K. Knie, G. Korschinek, W. Kutschera, A. Ofan, M. Paul, F. Quinto, G. Rugel, P. Steier, *Nature Communications* **2015**, 6 5956.
- [38] K. Hotokezaka, T. Piran, M. Paul, *Nature Physics* **2015**, 11 1042.
- [39] P. Macias, E. Ramirez-Ruiz, *ApJ* **2018**, 860, 2 89.
- [40] J. J. Cowan, C. Sneden, J. E. Lawler, A. Aprahamian, M. Wiescher, K. Langanke, G. Martínez-Pinedo, F.-K. Thielemann, *Reviews of Modern Physics* **2021**, 93, 1 015002.
- [41] K. Farouqi, F. K. Thielemann, S. Rosswog, K. L. Kratz, *A&A* **2022**, 663 A70.
- [42] J. M. Lattimer, D. N. Schramm, *ApJ, (Letters)* **1974**, 192 L145.
- [43] J. M. Lattimer, D. N. Schramm, *ApJ* **1976**, 210 549.
- [44] E. Symbalisty, D. N. Schramm, *Astrophys. Lett.* **1982**, 22 143.
- [45] D. Eichler, M. Livio, T. Piran, D. N. Schramm, *Nature* **1989**, 340 126.
- [46] S. Rosswog, F. K. Thielemann, M. B. Davies, W. Benz, T. Piran, In W. Hillebrandt, E. Müller, editors, *Nuclear Astrophysics*. Max-Planck-Institut für Physik und Astrophysik, Garching b. München, **1998** 103.
- [47] S. Rosswog, M. Liebendörfer, F.-K. Thielemann, M. Davies, W. Benz, T. Piran, *A & A* **1999**, 341 499.
- [48] C. Freiburghaus, S. Rosswog, F.-K. Thielemann, *ApJ* **1999**, 525 L121.
- [49] R. Oechslin, H. T. Janka, A. Marek, *A&A* **2007**, 467, 2 395.
- [50] A. Bauswein, T. W. Baumgarte, H.-T. Janka, *Physical Review Letters* **2013**, 111, 13 131101.
- [51] K. Hotokezaka, K. Kiuchi, K. Kyutoku, H. Okawa, Y.-i. Sekiguchi, M. Shibata, K. Taniguchi, *Phys. Rev. D* **2013**, 87, 2 024001.
- [52] D. Radice, A. Perego, K. Hotokezaka, S. A. Fromm, S. Bernuzzi, L. F. Roberts, *ApJ* **2018**, 869, 2 130.

Table 2: Fit coefficients (continued)

par. \ v_{ej}	Y_e	0.05c	0.1c	0.2c	0.3c	0.4c	0.5c	Y_e	0.05c	0.1c	0.2c	0.3c	0.4c	0.5c
$\dot{\epsilon}_0 \times 10^{18}$	0.25	20.0	25.0	40.0	38.0	58.0	70.0	0.3	6.1	18.0	47.1	47.1	74.8	74.8
α		1.44	1.40	1.46	1.66	1.60	1.60		1.36	1.33	1.33	1.33	1.374	1.374
t_0 (s)		0.65	0.38	0.22	0.18	0.12	0.095		0.540	0.31	0.18	0.13	0.095	0.081
σ (s)		0.05	0.030	0.025	0.045	0.05	0.05		0.11	0.04	0.021	0.021	0.017	0.017
α_1		8.00	8.00	5.00	7.50	7.00	6.50		4.5	3.8	4	4	4	4
t_1 (s)		0.080	0.060	0.065	0.028	0.020	0.015		0.14	0.123	0.089	0.060	0.045	0.031
σ_1 (s)		0.170	0.070	0.050	0.025	0.020	0.020		0.065	0.067	0.053	0.032	0.032	0.024
$\log C_1$		28.5	28.0	27.5	28.5	29.2	29.0		25.0	27.5	25.8	20.9	29.3	1.0
τ_1 (10^3 s)		4.77	4.77	4.77	4.77	4.07	4.07		4.77	4.77	28.2	1.03	0.613	1.0
$\log C_2$		22.0	22.8	23.0	23.0	23.5	23.5		10.0	0	0	19.8	22.0	21.0
τ_2 (10^5 s)		5.62	5.62	5.62	5.62	4.62	4.62		5.62	5.18	5.18	34.7	8.38	22.6
$\log C_3$		27.3	26.9	26.6	27.4	25.8	25.8		27.8	26.9	18.9	25.4	24.8	25.8
τ_3 (10^5 s)		0.18	0.18	0.18	0.18	0.32	0.32		0.12	0.18	50.8	0.18	0.32	0.32
$\dot{\epsilon}_0 \times 10^{18}$	0.35	7.3	7	16.3	23.2	43.2	150	0.4	0.0032	0.0032	0.008	0.007	0.009	0.015
α		1.40	1.358	1.384	1.384	1.384	1.344		1.80	1.80	2.10	2.10	1.90	1.90
t_0 (s)		0.385	0.235	0.1	0.06	0.035	0.025		26.0	26.0	0.4	0.4	0.12	-20
σ (s)		0.10	0.094	0.068	0.05	0.03	0.01		45	45	45	45	25	40
α_1		2.4	3.8	3.8	3.21	2.91	3.61		-1.55	-1.55	-0.75	-0.75	-2.50	-5.00
t_1 (s)		0.264	0.1	0.07	0.055	0.042	0.033		1.0	1.0	1.0	1.0	0.02	0.01
σ_1 (s)		0.075	0.044	0.03	0.02	0.02	0.014		10.0	10.0	10.0	10.0	0.02	0.01
$\log C_1$		28.7	27.0	28.0	28.0	27.4	25.3		28.5	29.1	29.5	30.1	30.4	29.9
τ_1 (10^3 s)		3.4	14.5	11.4	14.3	13.3	13.3		2.52	2.52	2.52	2.52	2.52	2.52
$\log C_2$		26.2	14.1	18.8	19.1	23.8	19.2		25.4	25.4	25.8	26.0	26.0	25.8
τ_2 (10^5 s)		0.15	4.49	95.0	95.0	0.95	146		0.12	0.12	0.12	0.12	0.12	0.14
$\log C_3$		22.8	17.9	18.9	25.4	24.8	25.5		20.6	20.2	19.8	19.2	19.5	18.4
τ_3 (10^5 s)		2.4	51.8	50.8	0.18	0.32	0.32		3.0	2.5	2.4	2.4	2.4	60.4
$\dot{\epsilon}_0 \times 10^{18}$	0.45	0.20	0.20	0.60	1.50	1.50	1.50	0.5	0.40	1.00	2.00	3.00	3.00	3.00
α		8.00	8.00	7.00	7.00	7.00	7.00		1.40	1.40	1.40	1.60	1.60	1.60
t_0 (s)		0.20	0.12	0.05	0.03	0.025	0.021		0.16	0.08	0.04	0.02	0.018	0.016
σ (s)		0.20	0.12	0.05	0.03	0.025	0.021		0.03	0.015	0.007	0.01	0.009	0.007
α_1		-1.55	-1.55	-1.55	-1.55	-1.55	-1.55		3.00	3.00	3.00	3.00	3.00	3.00
t_1 (s)		1.0	1.0	1.0	1.0	1.0	1.0		0.04	0.02	0.01	0.002	0.002	0.002
σ_1 (s)		10.0	10.0	10.0	10.0	10.0	10.0		0.01	0.005	0.002	10^{-4}	10^{-4}	10^{-4}
$\log C_1$		20.4	20.6	20.8	20.9	20.9	21.0		29.9	30.1	30.1	30.2	30.3	30.3
τ_1 (10^3 s)		1.02	1.02	1.02	1.02	1.02	1.02		0.22	0.22	0.22	0.22	0.22	0.22
$\log C_2$		18.4	18.4	18.6	18.6	18.6	18.6		27.8	28.0	28.2	28.2	28.3	28.3
τ_2 (10^5 s)		0.32	0.32	0.32	0.32	0.32	0.32		0.02	0.02	0.02	0.02	0.02	0.02
$\log C_3$		12.6	13.1	14.1	14.5	14.5	14.5		24.3	24.2	24.0	24.0	24.0	23.9
τ_3 (10^5 s)		200	200	200	200	200	200		8.76	8.76	8.76	8.76	8.76	8.76

- [53] V. Nedora, S. Bernuzzi, D. Radice, B. Daszuta, A. Endrizzi, A. Perego, A. Prakash, M. Safarzadeh, F. Schianchi, D. Logoteta, *ApJ* **2021**, *906*, 2 98.
- [54] L. Dessart, C. D. Ott, A. Burrows, S. Rosswog, E. Livne, *ApJ* **2009**, *690* 1681.
- [55] A. Perego, S. Rosswog, R. M. Cabezón, O. Korobkin, R. Käppeli, A. Arcones, M. Liebendörfer, *MNRAS* **2014**, *443* 3134.
- [56] D. M. Siegel, R. Ciolfi, L. Rezzolla, *ApJL* **2014**, *785* L6.
- [57] S. Fahlman, R. Fernández, *ApJ* **2018**, *869*, 1 L3.
- [58] S. Fujibayashi, M. Shibata, S. Wanajo, K. Kiuchi, K. Kyutoku, Y. Sekiguchi, *Phys. Rev. D* **2020**, *101*, 8 083029.
- [59] B. D. Metzger, A. L. Piro, E. Quataert, *MNRAS* **2008**, *390* 781.
- [60] A. M. Beloborodov, In M. Axelsson, editor, *American Institute of Physics Conference Series*, volume 1054 of *American Institute of Physics Conference Series*. **2008** 51–70.
- [61] W. H. Lee, E. Ramirez-Ruiz, D. López-Cámara, *ApJL* **2009**, *699* L93.
- [62] D. M. Siegel, B. D. Metzger, *ApJ* **2018**, *858*, 1 52.
- [63] R. Fernandez, A. Tchekhovskoy, E. Quataert, F. Foucart, D. Kasen, *MNRAS* **2019**, *482*, 3 3373.
- [64] J. M. Miller, B. R. Ryan, J. C. Dolence, A. Burrows, C. J. Fontes, C. L. Fryer, O. Korobkin, J. Lippuner, M. R. Mumpower, R. T. Wollaeger, *Phys. Rev. D* **2019**, *100*, 2 023008.
- [65] D. Radice, A. Perego, K. Hotokezaka, S. Bernuzzi, S. A. Fromm, L. F. Roberts, *ApJL* **2018**, *869*, 2 L35.
- [66] S. Fujibayashi, K. Kiuchi, N. Nishimura, Y. Sekiguchi, M. Shibata, *ApJ* **2018**, *860*, 1 64.
- [67] O. Korobkin, S. Rosswog, A. Arcones, C. Winteler, *MNRAS* **2012**, *426* 1940.
- [68] J. Lippuner, L. F. Roberts, *ApJ* **2015**, *815*, 2 82.
- [69] S. Rosswog, J. Sollerman, U. Feindt, A. Goobar, O. Korobkin, R. Wollaeger, C. Fremling, M. M. Kasliwal, *A&A* **2018**, *615* A132.
- [70] V. Nedora, S. Bernuzzi, D. Radice, A. Perego, A. Endrizzi, N. Ortiz, *ApJ Letters* **2019**, *886*, 2 L30.
- [71] S. Wanajo, Y. Sekiguchi, N. Nishimura, K. Kiuchi, K. Kyutoku, M. Shibata, *ApJL* **2014**, *789* L39.
- [72] O. Just, A. Bauswein, R. A. Pulpillo, S. Goriely, H.-T. Janka, *MNRAS* **2015**, *448* 541.
- [73] R. Fernandez, F. Foucart, D. Kasen, J. Lippuner, D. De-sai, L. F. Roberts, *ArXiv e-prints* **2016**.
- [74] C. Sneden, J. J. Cowan, R. Gallino, *Annual Review of Astronomy and Astrophysics* **2008**, *46* 241.
- [75] D. M. Siegel, *Nature Reviews Physics* **2022**, *4*, 5 306.
- [76] B. D. Metzger, *Living Reviews in Relativity* **2019**, *23*, 1 1.
- [77] R. Margutti, R. Chornock, *Annual Reviews of Astronomy and Astrophysics* **2021**, *59* 155.
- [78] E. Pian, *Frontiers in Astronomy and Space Sciences* **2021**, *7* 108.
- [79] M. Shibata, K. Hotokezaka, *Annual Review of Nuclear and Particle Science* **2019**, *69*, 1 annurev.
- [80] D. Radice, S. Bernuzzi, A. Perego, *Annual Review of Nuclear and Particle Science* **2020**, *70* 95.
- [81] B. P. Abbott, R. Abbott, T. D. Abbott, F. Acernese, K. Ackley, C. Adams, T. Adams, P. Addesso, R. X. Adhikari, V. B. Adya, et al., *Physical Review Letters* **2017**, *119*, 16 161101.
- [82] B. P. Abbott, R. Abbott, T. D. Abbott, F. Acernese, K. Ackley, C. Adams, T. Adams, P. Addesso, R. X. Adhikari, V. B. Adya, et al., *ApJL* **2017**, *848* L12.
- [83] K. Hotokezaka, K. Kyutoku, H. Okawa, M. Shibata, K. Kiuchi, *Phys. Rev. D* **2011**, *83*, 12 124008.
- [84] S. Köppel, L. Bovard, L. Rezzolla, *ApJL* **2019**, *872*, 1 L16.
- [85] S. Bernuzzi, M. Breschi, B. Daszuta, A. Endrizzi, D. Logoteta, V. Nedora, A. Perego, D. Radice, F. Schianchi, F. Zappa, I. Bombaci, N. Ortiz, *MNRAS* **2020**, *497*, 2 1488.
- [86] R. Kashyap, A. Das, D. Radice, S. Padamata, A. Prakash, D. Logoteta, A. Perego, D. A. Godzieba, S. Bernuzzi, I. Bombaci, F. J. Fattoyev, B. T. Reed, A. da Silva Schneider, *arXiv e-prints* **2021**, arXiv:2111.05183.
- [87] M. Shibata, K. Taniguchi, *Phys. Rev. D* **2006**, *73*, 6 064027.
- [88] K. Kiuchi, Y. Sekiguchi, M. Shibata, K. Taniguchi, *Phys. Rev. D* **2009**, *80*, 6 064037.
- [89] K. Hotokezaka, K. Kiuchi, K. Kyutoku, T. Muranushi, Y.-i. Sekiguchi, M. Shibata, K. Taniguchi, *Phys. Rev. D* **2013**, *88*, 4 044026.
- [90] T. M. Tauris, M. Kramer, P. C. C. Freire, N. Wex, H.-T. Janka, N. Langer, P. Podsiadlowski, E. Bozzo, S. Chaty, M. U. Kruckow, E. P. J. van den Heuvel, J. Antoniadis, R. P. Breton, D. J. Champion, *ApJ* **2017**, *846* 170.
- [91] K. Hotokezaka, K. Kiuchi, K. Kyutoku, H. Okawa, Y.-i. Sekiguchi, M. Shibata, K. Taniguchi, *Phys. Rev. D* **2013**, *87*, 2 024001.
- [92] A. Bauswein, S. Goriely, H.-T. Janka, *ApJ* **2013**, *773* 78.

- [93] S. Rosswog, P. Diener, F. Torsello, *Symmetry* **2022**, *14*, 6 1280.
- [94] T. Dietrich, M. Ujevic, *Classical and Quantum Gravity* **2017**, *34*, 10 105014.
- [95] D. Price, S. Rosswog, *Science* **2006**, *312* 719.
- [96] K. Kiuchi, P. Cerdá-Durán, K. Kyutoku, Y. Sekiguchi, M. Shibata, *Phys. Rev. D* **2015**, *92*, 12 124034.
- [97] C. Palenzuela, R. Aguilera-Miret, F. Carrasco, R. Ciolfi, J. V. Kalinani, W. Kastaun, B. Miñano, D. Viganò, *Phys. Rev. D* **2022**, *106*, 2 023013.
- [98] R. T. Wollaeger, C. L. Fryer, C. J. Fontes, J. Lippuner, W. T. Vestrand, M. R. Mumpower, O. Korobkin, A. L. Hungerford, W. P. Even, *ApJ* **2019**, *880*, 1 22.
- [99] Y. Sekiguchi, K. Kiuchi, K. Kyutoku, M. Shibata, K. Taniguchi, *ArXiv e-prints* **2016**.
- [100] S. Rosswog, *Royal Society of London Philosophical Transactions Series A* **2013**, *371* 20272.
- [101] L. Lehner, S. L. Liebling, C. Palenzuela, O. L. Caballero, E. O'Connor, M. Anderson, D. Neilsen, *Classical and Quantum Gravity* **2016**, *33*, 18 184002.
- [102] K. Kyutoku, K. Ioka, M. Shibata, *MNRAS* **2014**, *437*, 1 L6.
- [103] B. D. Metzger, A. Bauswein, S. Goriely, D. Kasen, *MNRAS* **2015**, *446* 1115.
- [104] C. Dean, R. Fernández, B. D. Metzger, *ApJ* **2021**, *921*, 2 161.
- [105] L. Combi, D. Siegel, *arXiv e-prints* **2022**, arXiv:2206.03618.
- [106] S. R. Kulkarni, *ArXiv Astrophysics e-prints* **2005**.
- [107] A. M. Beloborodov, C. Lundman, Y. Levin, *ApJ* **2020**, *897*, 2 141.
- [108] E. Nakar, T. Piran, *Nature* **2011**, *478* 82.
- [109] K. P. Mooley, E. Nakar, K. Hotokezaka, G. Hallinan, A. Corsi, D. A. Frail, A. Horesh, T. Murphy, E. Lenc, D. L. Kaplan, K. de, D. Dobie, P. Chandra, A. Deller, O. Gottlieb, M. M. Kasliwal, S. R. Kulkarni, S. T. Myers, S. Nissanke, T. Piran, C. Lynch, V. Bhalerao, S. Bourke, K. W. Bannister, L. P. Singer, *Nature* **2018**, *554* 207.
- [110] K. Hotokezaka, K. Kiuchi, M. Shibata, E. Nakar, T. Piran, *ApJ* **2018**, *867*, 2 95.
- [111] A. Hajela, R. Margutti, J. S. Bright, K. D. Alexander, B. D. Metzger, V. Nedora, A. Kathirgamaraju, B. Margalit, D. Radice, C. Guidorzi, E. Berger, A. MacFadyen, D. Giannios, R. Chornock, I. Heywood, L. Sironi, O. Gottlieb, D. Coppejans, T. Laskar, Y. Cendes, R. B. Duran, T. Eftekhari, W. Fong, A. McDowell, M. Nicholl, X. Xie, J. Zrake, S. Bernuzzi, F. S. Broekgaarden, C. D. Kilpatrick, G. Terreran, V. A. Villar, P. K. Blanchard, S. Gomez, G. Hosseinzadeh, D. J. Matthews, J. C. Rastinejad, *ApJL* **2022**, *927*, 1 L17.
- [112] L. Bildsten, C. Cutler, *ApJ* **1992**, *400* 175.
- [113] C. S. Kochanek, *ApJ* **1992**, *398* 234.
- [114] L. J. Papenfort, E. R. Most, S. Tootle, L. Rezzolla, *MNRAS* **2022**, *513*, 3 3646.
- [115] S. Rosswog, M. B. Davies, F.-K. Thielemann, T. Piran, *A&A* **2000**, *360* 171.
- [116] S. V. Chaurasia, T. Dietrich, M. Ujevic, K. Hendriks, R. Dudi, F. M. Fabbri, W. Tichy, B. Brügmann, *Phys. Rev. D* **2020**, *102*, 2 024087.
- [117] S. Rosswog, P. Diener, *Classical and Quantum Gravity* **2021**, *38*, 11 115002.
- [118] P. Diener, S. Rosswog, F. Torsello, *European Journal of Physics A, Volume 58, Issue 4, article id.74* **2022**.
- [119] S. Rosswog, *Cambridge University Press* **2022**, arXiv:2201.05896.
- [120] Y.-Z. Qian, S. E. Woosley, *ApJ* **1996**, *471* 331.
- [121] G. Martínez-Pinedo, T. Fischer, A. Lohs, L. Huther, *Phys. Rev. Lett.* **2012**, *109*, 25 251104.
- [122] D. Martin, A. Perego, A. Arcones, F.-K. Thielemann, O. Korobkin, S. Rosswog, *ApJ* **2015**, *813* 2.
- [123] R. Ciolfi, J. V. Kalinani, *ApJ Letters* **2020**, *900*, 2 L35.
- [124] P. A. Evans, S. B. Cenko, J. A. Kennea, S. W. K. Emery, N. P. M. Kuin, O. Korobkin, R. T. Wollaeger, C. L. Fryer, K. K. Madsen, F. A. Harrison, Y. Xu, E. Nakar, K. Hotokezaka, A. Lien, S. Campana, S. R. Oates, E. Troja, A. A. Breeveld, F. E. Marshall, S. D. Barthelmy, A. P. Beardmore, D. N. Burrows, G. Cusumano, A. D'Ai, P. D'Avanzo, V. D'Elia, M. de Pasquale, W. P. Even, C. J. Fontes, K. Forster, J. Garcia, P. Giommi, B. Grefenstette, C. Gronwall, D. H. Hartmann, M. Heida, A. L. Hungerford, M. M. Kasliwal, H. A. Krimm, A. J. Levan, D. Malesani, A. Melandri, H. Miyasaka, J. A. Nousek, P. T. O'Brien, J. P. Osborne, C. Pagani, K. L. Page, D. M. Palmer, M. Perri, S. Pike, J. L. Racusin, S. Rosswog, M. H. Siegel, T. Sakamoto, B. Sbarufatti, G. Tagliaferri, N. R. Tanvir, A. Tohuavohu, *Science* **2017**, *358* 1565.
- [125] M. Nicholl, E. Berger, D. Kasen, B. D. Metzger, J. Elias, C. Briceño, K. D. Alexander, P. K. Blanchard, R. Chornock, P. S. Cowperthwaite, T. Eftekhari, W. Fong, R. Margutti, V. A. Villar, P. K. G. Williams, W. Brown, J. Annis, A. Bahramian, D. Brout, D. A. Brown, H.-Y. Chen, J. C. Clemens, E. Denny, B. Dunlap, D. E. Holz, E. Marchesini, F. Massaro, N. Moskowitz, I. Pelisoli, A. Rest, F. Ricci, M. Sako, M. Soares-Santos, J. Strader, *ApJL* **2017**, *848* L18.

- [126] C. McCully, D. Hiramatsu, D. A. Howell, G. Hosseinzadeh, I. Arcavi, D. Kasen, J. Barnes, M. M. Shara, T. B. Williams, P. Väisänen, S. B. Potter, E. Romero-Colmenero, S. M. Crawford, D. A. H. Buckley, J. Cooke, I. Andreoni, T. A. Pritchard, J. Mao, M. Gromadzki, J. Burke, *ApJL* **2017**, *848* L32.
- [127] B. D. Metzger, T. A. Thompson, E. Quataert, *ApJ* **2018**, *856* 101.
- [128] O. Korobkin, R. T. Wollaeger, C. L. Fryer, A. L. Hungerford, S. Rosswog, C. J. Fontes, M. R. Mumpower, E. A. Chase, W. P. Even, J. Miller, G. W. Misch, J. Lippuner, *ApJ* **2021**, *910*, 2 116.
- [129] P. S. Cowperthwaite, E. Berger, V. A. Villar, B. D. Metzger et al., *ApJL* **2017**, *848* L17.
- [130] A. M. Beloborodov, *ApJ* **2003**, *588*, 2 931.
- [131] N. Kawanaka, S. Mineshige, *ApJ* **2007**, *662*, 2 1156.
- [132] W. Chen, A. M. Beloborodov, *ApJ* **2007**, *657* 383.
- [133] B. D. Metzger, A. L. Piro, E. Quataert, *MNRAS* **2009**, *396* 304.
- [134] I. U. Roederer, J. J. Cowan, A. I. Karakas, K.-L. Kratz, M. Lugaro, J. Simmerer, K. Farouqi, C. Sneden, *ApJ* **2010**, *724*, 2 975.
- [135] E. M. Holmbeck, T. C. Beers, I. U. Roederer, V. M. Placco, T. T. Hansen, C. M. Sakari, C. Sneden, C. Liu, Y. S. Lee, J. J. Cowan, A. Frebel, *ApJ* **2018**, *859* L24.
- [136] E. M. Holmbeck, T. M. Sprouse, M. R. Mumpower, N. Vassh, R. Surman, T. C. Beers, T. Kawano, *ApJ* **2019**, *870* 23.
- [137] M.-R. Wu, I. Tamborra, O. Just, H.-T. Janka, *Phys. Rev. D* **2017**, *96*, 12 123015.
- [138] M. Eichler, W. Sayar, A. Arcones, T. Rauscher, *ApJ* **2019**, *879*, 1 47.
- [139] E. M. Holmbeck, A. Frebel, G. C. McLaughlin, M. R. Mumpower, T. M. Sprouse, R. Surman, *ApJ* **2019**, *881* 5.
- [140] J. M. Miller, B. R. Ryan, J. C. Dolence, *ApJS* **2019**, *241*, 2 30.
- [141] O. Just, S. Goriely, H. T. Janka, S. Nagataki, A. Bauswein, *MNRAS* **2022**, *509*, 1 1377.
- [142] I. V. Artemova, G. Bjoernsson, I. D. Novikov, *ApJ* **1996**, *461* 565.
- [143] R. Fernández, F. Foucart, J. Lippuner, *MNRAS* **2020**, *497*, 3 3221.
- [144] B. P. Abbott, R. Abbott, T. D. Abbott, F. Acernese, K. Ackley, C. Adams, T. Adams, P. Addesso, R. X. Adhikari, V. B. Adya, et al., *Physical Review Letters* **2017**, *119*, 16 161101.
- [145] L.-X. Li, B. Paczyński, *ApJL* **1998**, *507* L59.
- [146] B. D. Metzger, G. Martinez-Pinedo, S. Darbha, E. Quataert, A. Arcones, D. Kasen, R. Thomas, P. Nugent, I. V. Panov, N. T. Zinner, *MNRAS* **2010**, *406* 2650.
- [147] D. Kasen, N. R. Badnell, J. Barnes, *ApJ* **2013**, *774* 25.
- [148] M. Tanaka, K. Hotokezaka, *ApJ* **2013**, *775* 113.
- [149] C. J. Fontes, C. L. Fryer, A. L. Hungerford, P. Hakel, J. Colgan, D. P. Kilcrease, M. E. Sherrill, *High Energy Density Physics* **2015**, *16* 53.
- [150] D. Kasen, B. Metzger, J. Barnes, E. Quataert, E. Ramirez-Ruiz, *Nature* **2017**, *551* 80.
- [151] C. J. Fontes, C. L. Fryer, A. L. Hungerford, R. T. Wollaeger, S. Rosswog, E. Berger, *ArXiv e-prints* **2017**.
- [152] W. Even, O. Korobkin, C. L. Fryer, C. J. Fontes, R. T. Wollaeger, A. Hungerford, J. Lippuner, J. Miller, M. R. Mumpower, G. W. Misch, *ApJ* **2020**, *899*, 1 24.
- [153] R. T. Wollaeger, O. Korobkin, C. J. Fontes, S. K. Rosswog, W. P. Even, C. L. Fryer, J. Sollerman, A. L. Hungerford, D. R. van Rossum, A. B. Wollaber, *MNRAS* **2018**, *478* 3298.
- [154] C. J. Fontes, C. L. Fryer, A. L. Hungerford, R. T. Wollaeger, O. Korobkin, *MNRAS* **2020**, *493*, 3 4143.
- [155] K. Hotokezaka, M. Tanaka, D. Kato, G. Gaigalas, *MNRAS* **2021**, *506*, 4 5863.
- [156] Q. Pognan, A. Jerkstrand, J. Grumer, *MNRAS* **2022**, *513*, 4 5174.
- [157] Q. Pognan, A. Jerkstrand, J. Grumer, *MNRAS* **2022**, *510*, 3 3806.
- [158] R. Chornock, E. Berger, D. Kasen, P. S. Cowperthwaite, M. Nicholl, V. A. Villar, K. D. Alexander, P. K. Blanchard, T. Eftekhari, W. Fong, R. Margutti, P. K. G. Williams, J. Annis, D. Brout, D. A. Brown, H.-Y. Chen, M. R. Drout, B. Farr, R. J. Foley, J. A. Frieman, C. L. Fryer, K. Herner, D. E. Holz, R. Kessler, T. Matheson, B. D. Metzger, E. Quataert, A. Rest, M. Sako, D. M. Scolnic, N. Smith, M. Soares-Santos, *ApJL* **2017**, *848* L19.
- [159] E. Pian, P. D’Avanzo, S. Benetti, M. Branchesi, E. Brocato, S. Campana, E. Cappellaro, S. Covino, V. D’Elia, J. P. U. Fynbo, F. Getman, G. Ghirlanda, G. Ghisellini, A. Grado, G. Greco, J. Hjorth, C. Kouveliotou, A. Levan, L. Limatola, D. Malesani, P. A. Mazzali, A. Melandri, P. Møller, L. Nicastro, E. Palazzi, S. Piranomonte, A. Rossi, O. S. Salafia, J. Selsing, G. Stratta, M. Tanaka, N. R. Tanvir, L. Tomasella, D. Watson, S. Yang, L. Amati, L. A. Antonelli, S. Ascenzi, M. G. Bernardini, M. Boër, F. Bufano, A. Bulgarelli, M. Capaccioli, P. Casella, A. J. Castro-Tirado, E. Chassande-Mottin, R. Ciolfi, C. M. Copperwheat, M. Dadina, G. De Cesare, A. di Paola, Y. Z. Fan, B. Gendre, G. Giuffrida, A. Giunta, L. K. Hunt, G. L. Israel, Z.-P. Jin, M. M. Kasliwal, S. Klose,

- M. Lisi, F. Longo, E. Maiorano, M. Mapelli, N. Masetti, L. Nava, B. Patricelli, D. Perley, A. Pescalli, T. Piran, A. Possenti, L. Pulone, M. Razzano, R. Salvaterra, P. Schipani, M. Spera, A. Stamerra, L. Stella, G. Tagliiferri, V. Testa, E. Troja, M. Turatto, S. D. Vergani, D. Vergani, *Nature* **2017**, *551* 67.
- [160] N. R. Tanvir, A. J. Levan, C. González-Fernández, O. Korobkin, I. Mandel, S. Rosswog, J. Hjorth, P. D'Avanzo, A. S. Fruchter, C. L. Fryer, T. Kangas, B. Milvang-Jensen, S. Rosetti, D. Steeghs, R. T. Wollaeger, Z. Cano, C. M. Copperwheat, S. Covino, V. D'Elia, A. de Ugarte Postigo, P. A. Evans, W. P. Even, S. Fairhurst, R. Figuera Jaimes, C. J. Fontes, Y. I. Fujii, J. P. U. Fynbo, B. P. Gompertz, J. Greiner, G. Hodosan, M. J. Irwin, P. Jakobsson, U. G. Jørgensen, D. A. Kann, J. D. Lyman, D. Malesani, R. G. McMahon, A. Melandri, P. T. O'Brien, J. P. Osborne, E. Palazzi, D. A. Perley, E. Pian, S. Piranomonte, M. Rabus, E. Rol, A. Rowlinson, S. Schulze, P. Sutton, C. C. Thöne, K. Ulaczyk, D. Watson, K. Wiersema, R. A. M. J. Wijers, *ApJL* **2017**, *848* L27.
- [161] K. Kawaguchi, M. Shibata, M. Tanaka, *ApJ* **2018**, *865* L21.
- [162] A. L. Piro, J. A. Kollmeier, *ApJ* **2018**, *855*, 2 103.
- [163] S. Kisaka, K. Ioka, E. Nakar, *ApJ* **2016**, *818*, 2 104.
- [164] E. Troja, L. Piro, H. van Eerten, R. T. Wollaeger, M. Im, O. D. Fox, N. R. Butler, S. B. Cenko, T. Sakamoto, C. L. Fryer, R. Ricci, A. Lien, R. E. Ryan, O. Korobkin, S. K. Lee, many more, *Nature* **2017**, *551*, 7678 71.
- [165] M. M. Kasliwal, E. Nakar, L. P. Singer, D. L. Kaplan, et al., *Science* **2017**, *358* 1559.
- [166] D. Watson, C. J. Hansen, J. Selsing, A. Koch, D. B. Malesani, A. C. Andersen, J. P. U. Fynbo, A. Arcones, A. Bauswein, S. Covino, A. Grado, K. E. Heintz, L. Hunt, C. Kouveliotou, G. Leloudas, A. J. Levan, P. Mazzali, E. Pian, *Nature* **2019**, *574*, 7779 497.
- [167] N. Domoto, M. Tanaka, S. Wanaajo, K. Kawaguchi, *ApJ* **2021**, *913*, 1 26.
- [168] J. H. Gillanders, M. McCann, S. A. Sim, S. J. Smartt, C. P. Ballance, *MNRAS* **2021**, *506*, 3 3560.
- [169] J. H. Gillanders, S. J. Smartt, S. A. Sim, A. Bauswein, S. Goriely, *MNRAS* **2022**.
- [170] A. Perego, D. Vescovi, A. Fiore, L. Chiesa, C. Vogl, S. Benetti, S. Bernuzzi, M. Branchesi, E. Cappellaro, S. Cristallo, A. Flörs, W. E. Kerzendorf, D. Radice, *ApJ* **2022**, *925*, 1 22.
- [171] M. R. Drout, A. L. Piro, B. J. Shappee, C. D. Kilpatrick, J. D. Simon, C. Contreras, D. A. Coulter, R. J. Foley, M. R. Siebert, N. Morrell, K. Boutsia, F. Di Mille, T. W.-S. Holoiën, D. Kasen, J. A. Kollmeier, B. F. Madore, A. J. Monson, A. Murguia-Berthier, Y.-C. Pan, J. X. Prochaska, E. Ramirez-Ruiz, A. Rest, C. Adams, K. Alatalo, E. Bañados, J. Baughman, T. C. Beers, R. A. Bernstein, T. Bitsakis, A. Campillay, T. T. Hansen, C. R. Higgs, A. P. Ji, G. Maravelias, J. L. Marshall, C. Moni Bidin, J. L. Prieto, K. C. Rasmussen, C. Rojas-Bravo, A. L. Strom, N. Ulloa, J. Vargas-González, Z. Wan, D. D. Whitten, *Science, in press*, available via doi:10.1126/science.aaq0049 **2017**.
- [172] M.-R. Wu, J. Barnes, G. Martínez-Pinedo, B. D. Metzger, *Phys. Rev. Lett.* **2019**, *122*, 6 062701.
- [173] M. M. Kasliwal, D. Kasen, R. M. Lau, D. A. Perley, S. Rosswog, E. O. Ofek, K. Hotokezaka, R.-R. Chary, J. Sollerman, A. Goobar, D. L. Kaplan, *MNRAS* **2022**, *510*, 1 L7.
- [174] V. A. Villar, P. S. Cowperthwaite, E. Berger, P. K. Blanchard, S. Gomez, K. D. Alexander, R. Margutti, R. Chornock, T. Eftekhari, G. G. Fazio, J. Guillochon, J. L. Hora, M. Nicholl, P. K. G. Williams, *ApJL* **2018**, *862*, 1 L11.
- [175] N. Domoto, M. Tanaka, D. Kato, K. Kawaguchi, K. Hotokezaka, S. Wanaajo, *arXiv e-prints* **2022**, arXiv:2206.04232.
- [176] B. J. Shappee, J. D. Simon, M. R. Drout, A. L. Piro, N. Morrell, J. L. Prieto, D. Kasen, T. W.-S. Holoiën, J. A. Kollmeier, D. D. Kelson, D. A. Coulter, R. J. Foley, C. D. Kilpatrick, M. R. Siebert, B. F. Madore, A. Murguia-Berthier, Y.-C. Pan, J. X. Prochaska, E. Ramirez-Ruiz, A. Rest, C. Adams, K. Alatalo, E. Bañados, J. Baughman, R. A. Bernstein, T. Bitsakis, K. Boutsia, J. R. Bravo, F. Di Mille, C. R. Higgs, A. P. Ji, G. Maravelias, J. L. Marshall, V. M. Placco, G. Prieto, Z. Wan, *Science* **2017**, *358* 1574.
- [177] V. A. Villar, J. Guillochon, E. Berger, B. D. Metzger, P. S. Cowperthwaite, M. Nicholl, K. D. Alexander, P. K. Blanchard, R. Chornock, T. Eftekhari, W. Fong, R. Margutti, P. K. G. Williams, *ApJL* **2017**, *851* L21.
- [178] A. Perego, D. Radice, S. Bernuzzi, *ArXiv e-prints* **2017**.
- [179] E. Waxman, E. O. Ofek, D. Kushnir, A. Gal-Yam, *MNRAS* **2018**, *481*, 3 3423.
- [180] K. Hotokezaka, M. Tanaka, D. Kato, G. Gaigalas, *arXiv e-prints* **2022**, arXiv:2204.00737.
- [181] K. Hotokezaka, E. Nakar, *ApJ* **2020**, *891*, 2 152.
- [182] A. P. Ji, M. R. Drout, T. T. Hansen, *ApJ* **2019**, *882*, 1 40.
- [183] M. Arnould, S. Goriely, K. Takahashi, *Phys. Reports* **2007**, *450* 97.
- [184] J. Abadie, B. P. Abbott, R. Abbott, M. Abernathy, T. Accadia, F. Acernese, C. Adams, R. Adhikari, P. Ajith, B. Allen, et al., *Classical and Quantum Gravity* **2010**, *27*, 17 173001.
- [185] R. Abbott et al., *arXiv e-prints* **2021**, arXiv:2111.03634.

- [186] S. Dichiaro, E. Troja, B. O'Connor, F. E. Marshall, P. Beniamini, J. K. Cannizzo, A. Y. Lien, T. Sakamoto, *MNRAS* **2020**, *492*, 4 5011.
- [187] K. Grunthal, M. Kramer, G. Desvignes, *MNRAS* **2021**, *507*, 4 5658.
- [188] R. K. Kopparapu, C. Hanna, V. Kalogera, R. O'Shaughnessy, G. González, P. R. Brady, S. Fairhurst, *ApJ* **2008**, *675*, 2 1459.
- [189] I. Mandel, F. S. Broekgaarden, *Living Reviews in Relativity* **2022**, *25*, 1 1.
- [190] A. Perego, S. Bernuzzi, D. Radice, *European Physical Journal A* **2019**, *55*, 8 124.
- [191] S. Rosswog, O. Korobkin, A. Arcones, F.-K. Thielemann, T. Piran, *MNRAS* **2014**, *439* 744.
- [192] Z. Wu, G. Ricigliano, R. Kashyap, A. Perego, D. Radice, *MNRAS* **2022**, *512*, 1 328.
- [193] S. Darbha, D. Kasen, F. Foucart, D. J. Price, *ApJ* **2021**, *915*, 1 69.
- [194] A. R. Stewart, L.-T. Lo, O. Korobkin, I. Sagert, J. Loiseau, H. Lim, M. A. Kaltenborn, C. M. Mauney, J. Maxwell Miller, *arXiv e-prints* **2022**, arXiv:2201.01865.
- [195] S. Fujibayashi, K. Kiuchi, S. Wanajo, K. Kyutoku, Y. Sekiguchi, M. Shibata, *arXiv e-prints* **2022**, arXiv:2205.05557.
- [196] P. Meszaros, *Reports of Progress in Physics* **2006**, *69* 2259.
- [197] E. Nakar, *Phys. Rep.* **2007**, *442* 166.
- [198] W. H. Lee, E. Ramirez-Ruiz, *New Journal of Physics* **2007**, *9* 17.
- [199] P. Kumar, B. Zhang, *Phys. Rep.* **2015**, *561* 1.
- [200] P. Mösta, D. Radice, R. Haas, E. Schnetter, S. Bernuzzi, *ApJL* **2020**, *901*, 2 L37.
- [201] V. V. Usov, *Nature* **1992**, *357* 472.
- [202] H. Nagakura, K. Hotokezaka, Y. Sekiguchi, M. Shibata, K. Ioka, *ApJL* **2014**, *784*, 2 L28.
- [203] A. Murguia-Berthier, E. Ramirez-Ruiz, G. Montes, F. De Colle, L. Rezzolla, S. Rosswog, K. Takami, A. Perego, W. H. Lee, *ArXiv e-prints* **2016**.
- [204] D. Lazzati, A. Deich, B. J. Morsony, J. C. Workman, *MNRAS* **2017**, *471*, 2 1652.
- [205] O. Gottlieb, E. Nakar, T. Piran, *MNRAS* **2018**, *473* 576.
- [206] J. D. Lyman, G. P. Lamb, A. J. Levan, I. Mandel, N. R. Tanvir, S. Kobayashi, B. Gompertz, J. Hjorth, A. S. Fruchter, T. Kangas, D. Steeghs, I. A. Steele, Z. Cano, C. Copperwheat, P. A. Evans, J. P. U. Fynbo, C. Gall, M. Im, L. Izzo, P. Jakobsson, B. Milvang-Jensen, P. O'Brien, J. P. Osborne, E. Palazzi, D. A. Perley, E. Pian, S. Rosswog, A. Rowlinson, S. Schulze, E. R. Stanway, P. Sutton, C. C. Thöne, A. de Ugarte Postigo, D. J. Watson, K. Wiersema, R. A. M. J. Wijers, *Nature Astronomy* **2018**, *2* 751.
- [207] K. P. Mooley, A. T. Deller, O. Gottlieb, E. Nakar, G. Hallinan, S. Bourke, D. A. Frail, A. Horesh, A. Corsi, K. Hotokezaka, *ArXiv e-prints* **2018**.
- [208] L. Nativi, M. Bulla, S. Rosswog, C. Lundman, G. Kowal, D. Gizzi, G. P. Lamb, A. Perego, *MNRAS* **2021**, *500*, 2 1772.
- [209] L. Nativi, G. P. Lamb, S. Rosswog, C. Lundman, G. Kowal, *arXiv e-prints* **2021**, arXiv:2109.00814.
- [210] A. Murguia-Berthier, E. Ramirez-Ruiz, F. De Colle, A. Janiuk, S. Rosswog, W. H. Lee, *ApJ* **2021**, *908*, 2 152.
- [211] D. Kasen, R. Fernández, B. D. Metzger, *MNRAS* **2015**, *450* 1777.
- [212] R. T. Wollaeger, O. Korobkin, C. J. Fontes, S. K. Rosswog, W. P. Even, C. L. Fryer, J. Sollerman, A. L. Hungerford, D. R. van Rossum, A. B. Wollaber, *MNRAS* **2018**, *478*, 3 3298.
- [213] J. Heinzl, M. W. Coughlin, T. Dietrich, M. Bulla, S. Antier, N. Christensen, D. A. Coulter, R. J. Foley, L. Issa, N. Khetan, *MNRAS* **2021**, *502*, 2 3057.
- [214] D. Grossman, O. Korobkin, S. Rosswog, T. Piran, *MNRAS* **2014**, *439* 757.
- [215] S. Darbha, D. Kasen, *ApJ* **2020**, *897*, 2 150.
- [216] X. Li, D. M. Siegel, *Phys. Rev. Lett.* **2021**, *126*, 25 251101.
- [217] M. Bulla, K. Kyutoku, M. Tanaka, S. Covino, J. R. Bruten, T. Matsumoto, J. R. Maund, V. Testa, K. Wiersema, *MNRAS* **2021**, *501*, 2 1891.
- [218] Y. Zhu, R. T. Wollaeger, N. Vassh, R. Surman, T. M. Sprouse, M. R. Mumpower, P. Möller, G. C. McLaughlin, O. Korobkin, T. Kawano, P. J. Jaffke, E. M. Holmbeck, C. L. Fryer, W. P. Even, A. J. Couture, J. Barnes, *ApJL* **2018**, *863*, 2 L23.
- [219] K. Hotokezaka, R. Sari, T. Piran, *MNRAS* **2017**, *468* 91.
- [220] J. Barnes, D. Kasen, M.-R. Wu, G. Martinez-Pinedo, *ApJ* **2016**, *829* 110.
- [221] K. Hotokezaka, E. Nakar, *ApJ* **2020**, *891*, 2 152.
- [222] E. Waxman, E. O. Ofek, D. Kushnir, *ApJ* **2019**, *878*, 2 93.

- [223] C. Winteler, Ph.D. thesis, University Basel, CH, **2012**.
- [224] C. Winteler, R. Käppeli, A. Perego, A. Arcones, N. Vasset, N. Nishimura, M. Liebendörfer, F.-K. Thielemann, *ApJL* **2012**, 750 L22.
- [225] F.-K. Thielemann, A. Arcones, R. Käppeli, M. Liebendörfer, T. Rauscher, C. Winteler, C. Fröhlich, I. Dillmann, T. Fischer, G. Martinez-Pinedo, K. Langanke, K. Farouqi, K.-L. Kratz, I. Panov, I. K. Korneev, *Progress in Particle and Nuclear Physics* **2011**, 66 346.
- [226] T. Rauscher, F.-K. Thielemann, *Atomic Data and Nuclear Data Tables* **2000**, 75 1.
- [227] P. Möller, J. R. Nix, W. D. Myers, W. J. Swiatecki, *At. Data Nucl. Data Tables* **1995**, 59 185.
- [228] G. M. Fuller, W. A. Fowler, M. J. Newman, *ApJS* **1982**, 48 279.
- [229] K. Langanke, G. Martinez-Pinedo, *Atomic Data and Nuclear Data Tables* **2001**, 79 1.
- [230] I. V. Panov, I. Y. Korneev, T. Rauscher, G. Martinez-Pinedo, A. Kelić-Heil, N. T. Zinner, F.-K. Thielemann, *A & A* **2010**, 513 A61.
- [231] I. V. Panov, E. Kolbe, B. Pfeiffer, T. Rauscher, K.-L. Kratz, F.-K. Thielemann, *Nuclear Physics A* **2005**, 747 633.
- [232] C. Freiburghaus, J. Rembges, T. Rauscher, E. Kolbe, F.-K. Thielemann, K.-L. Kratz, J. Cowan, *ApJ* **1999**, 516 381.
- [233] R. Fernandez, E. Quataert, J. Schwab, D. Kasen, S. Rosswog, *MNRAS* **2015**, 449 390.